Magnetostratigraphy of the Triassic Moenkopi Formation From the Continuous Cores Recovered in Colorado Plateau Coring Project Phase 1 (CPCP-1), Petrified Forest National Park, Arizona, USA: Correlation of the Early to Middle Triassic Strata and Biota in Colorado Plateau and Its Environs

Ziaul Haque[1] , John W. Geissman[1,2] , Randall B. Irmis[3,4], Paul E. Olsen[5], Christopher Lepre[5,6] , Hesham Buhedma[1], Roland Mundil[7], William G. Parker[8] , Cornelia Rasmussen[9] , and George E. Gehrels[10]

[1]Department of Geosciences, University of Texas at Dallas, Richardson, TX, USA, [2]Department of Earth & Planetary Sciences, University of New Mexico, Albuquerque, NM, USA, [3]Department of Geology & Geophysics, University of Utah, Salt Lake City, UT, USA, [4]Natural History Museum of Utah, University of Utah, Salt Lake City, UT, USA, [5]Lamont-Doherty Earth Observatory of Columbia University, Palisades, NY, USA, [6]Earth & Planetary Sciences, Rutgers University, Piscataway, NJ, USA, [7]Berkeley Geochronology Center, Berkeley, CA, USA, [8]Petrified Forest National Park, Petrified Forest, AZ, USA, [9]Institute for Geophysics, Jackson School of Geosciences, University of Texas at Austin, Austin, TX, USA, [10]Department of Geosciences, University of Arizona, Tucson, AZ, USA

Abstract The Colorado Plateau Coring Project Phase 1 (CPCP-1) acquired three continuous drill cores from Petrified Forest National Park (PFNP), Arizona, U.S.A., two of which (CPCP-PFNP13-1A and CPCP-PFNP13-2B) intersected the Upper Triassic Chinle Formation, Lower(?)-Middle Triassic Moenkopi Formation (MF) and Permian Coconino Sandstone. We examined both cores to construct a high-resolution magnetostratigraphy of MF strata, and progressive demagnetization data yield well-defined, interpretable paleomagnetic results. Each lithostratigraphic member of the MF (Wupatki, Moqui, and Holbrook members) contains authigenic and detrital hematite as the dominant magnetic carrier with distinguishing rock magnetic characteristics. Magnetostratigraphy of MF strata in both CPCP-1 cores consists of six normal and six reverse polarity magnetozones, from the youngest to the oldest, MF1n to MF6r. Recent single-crystal chemical abrasion–thermal ionization mass spectrometry (CA-TIMS) U-Pb data from a sample in magnetozone MF1n yield a latest Anisian/earliest Ladinian (241.38 $\pm$ 0.43 Ma) age. Correlation of the CA-TIMS-calibrated magnetostratigraphy with the astronomically tuned polarity timescale for the Middle Triassic deep-marine Guandao (GD) section of South China ties the magnetozone MF1n with GD8 and MF6r with GD2r, and implies that the MF spans, at most, the earliest Anisian (Aegean) to latest Anisian (Illyrian)/earliest Ladinian stages (ca. 246.8 to 241.5 Ma). This age estimate for the MF suggests that the timespan of the regional, pre-Norian disconformity is about 17 Ma, which demonstrates that MF vertebrate fossil assemblages in east-central Arizona are millions of years (minimally 3–4 Ma) younger than previously suggested and are all Anisian in age, with no indications of substantial hiatuses in the MF section.

Plain Language Summary The Triassic Period, between about 252 and 201.5 million years ago, witnessed many significant Earth System events, including extreme temperature swings, high atmospheric carbon-dioxide concentration, and biotic recovery from the Earth's greatest mass extinction at its beginning and another mass extinction at its end. This research is aimed at obtaining a high-resolution magnetic polarity stratigraphy for the Moenkopi Formation based on two cores recovered from the Petrified Forest National Park, Arizona, U.S.A., to provide a robust age constraint of its constituent fossil assemblages that will allow a correlation across continents, document key biotic events, such as the recovery from the end-Permian mass extinction, the diversification of reptiles, and the origin of dinosauromorphs. We have identified six magnetic reversal events during the deposition of the Moenkopi Formation rocks and suggest that these strata span, at most, ~246.8 Ma to ~241.5 Ma. This study also suggests that the time gap between the Moenkopi Formation and the overlying Chinle Formation, the

home of the petrified forests, is about 17 Ma long. The revised age model of the Moenkopi Formation from this study will provide a high-resolution age constraint for future paleoclimatic, biotic, and correlation studies of rocks from a similar age on a global basis.

1. Introduction

Bracketed between two of the largest mass extinctions in Earth history, the Triassic Period (ca. 252–201.5 Ma) experienced a succession of significant global events, including the origin of many modern animal lineages, high atmospheric pCO$_2$ concentration over prolonged time, extreme temperature swings, anoxic episodes, the northward translation of North America and initiation of the break-up of Pangea, and the first pulses of the emplacement of the Central Atlantic Magmatic Province (Blackburn et al., 2013; Mundil et al., 2004; Olsen et al., 2018; Payne et al., 2004; and Trotter et al., 2015). Early Mesozoic epicontinental basins of western North America preserve one of the world's paleontologically richest and well-studied Triassic and Jurassic nonmarine sedimentary sequences, which contain a spectacular record of the climatic, biotic, and tectonic development of western equatorial Pangea (Olsen et al., 2008). The rich biotic records of the Triassic and Jurassic strata preserved on the Colorado Plateau and environs have been of considerable interest for well over a century and have prompted efforts to place these strata into improved chronostratigraphic context (e.g., Gehrels et al., 2020; Irmis et al., 2011; Kent et al., 2018, 2019; Ramezani et al., 2005, 2011; Rasmussen et al., 2020; and Riggs et al., 2003). Despite the pivotal role of the Triassic Period in Earth history, until recently, the time interval had relatively sparse numerical age control (e.g., Ogg, 2012). To address this issue, an interdisciplinary multiphase coring experiment the "Colorado Plateau Coring Project Phase 1 (CPCP-1)" was initiated to develop a high-resolution timescale through independent, non-biostratigraphic means to facilitate detailed regional and global correlation based on magnetic polarity stratigraphy and U-Pb zircon geochronology (Olsen et al., 2008, 2018). Three cores were recovered as part of CPCP-1, which are: CPCP-PFNP13-1A from the northern part of the park; and about 30 km away, CPCP-PFNP13-2A and CPCP-PFNP13-2B from the southern part of the park, hereafter abbreviated as CPCP-1A, CPCP-2A, and CPCP-2B, respectively. The Newark–Hartford Astrochronostratigraphic polarity timescale (N-H APTS) had previously been developed to provide a robust time calibration for the Late Triassic and earliest Jurassic (Kent et al., 2017). The magnetostratigraphic age model constructed from the Upper Triassic Chinle Formation strata intersected in the CPCP-1 experiment is in good agreement with the N-H APTS for that part of the time interval (Kent et al., 2018, 2019; and Rasmussen et al., 2020). The maximum depositional age for the lowermost member (Mesa Redondo) of the Chinle Formation reported from the CPCP-1A core is ca. 224–225 Ma, based on coupled magnetochronology (Gehrels et al., 2020; and Kent et al., 2018, 2019) and CA-TIMS U-Pb age data (Rasmussen et al., 2020), which is an early Norian age.

Early research on the CPCP-1 core focused on the Upper Triassic Chinle Formation. In this study, we focus on the Lower (?) to Middle Triassic Moenkopi Formation that preserves important clues for biotic recovery and evolution from the end-Permian extinction. What have been inferred to be Early to Middle Triassic age strata on the Colorado Plateau comprise the Moenkopi Formation (Blakey & Gubitosa, 1983; McKee, 1954; Stewart et al., 1972), which is composed, in varying amounts, of red to yellowish-gray alternating siltstone, sandstone, mudstone, and limestone. In the Petrified Forest National Park (PFNP) region of northeastern Arizona, the Moenkopi Formation consists of thin-bedded reddish siltstone with interlayered fine to medium grained sandstone and mudstone and is subdivided into three members; the lower Wupatki Member, the middle Moqui Member, and the upper Holbrook Member (McKee, 1954; Nesbitt, 2005a; Stewart et al., 1972). Although it comprises one of the thinner Moenkopi sections, these outcrops in the drainage basin of the Little Colorado River preserve the richest and most-studied nonmarine nominally Early to Middle Triassic age macrofloral and vertebrate fossil assemblages from the whole of North America (e.g., Ash & Morales, 1993; Lucas & Schoch, 2002; Morales, 1987; Nesbitt, 2005a, 2005c; Peabody, 1948; Schoch, 2000; Welles, 1947; and Welles & Cosgriff, 1965). These fossil archives are an important record for understanding nonmarine recovery from the end-Permian mass extinction (e.g., Romano et al., 2020; Tarailo & Fastovsky, 2012) and have played a critical role in the biostratigraphic correlation of nonmarine units across Pangea (e.g., Colbert & Gregory, 1957; Lucas, 1998, 2010; Lucas & Schoch, 2002; Morales, 1987; Romano et al., 2020; and Welles & Cosgriff, 1965).

Despite the importance of this record, the depositional timespan represented by the Moenkopi Formation remains relatively poorly determined and age estimates are almost entirely derived from two sets of biostratigraphic data. The oldest age estimates for the Moenkopi Formation are Smithian-Spathian (Olenekian: Early Triassic) in age and are inferred from marine invertebrate fossils from two marine tongues (Timpoweap and Sinbad members, and Virgin Limestone) in strata exposed in southwestern and central Utah (e.g., Blakey, 1974; Hautmann et al., 2013; Lucas, Goodspeed, et al., 2007; Lucas, Krainer, et al., 2007; McKee, 1954; Poborski, 1954; and Stewart et al., 1972). In contrast, ages for sections in northern Arizona, including the youngest age estimates for the formation, are based on vertebrate biostratigraphic correlations to European sections suggesting a Spathian to early Anisian age (Lucas, 1998, 2010; Lucas & Schoch, 2002; Morales, 1987; Romano et al., 2020; and Welles & Cosgriff, 1965). Thus, most workers have reasoned that the Moenkopi Formation spans part of the Early to Middle Triassic, but the formation could conceivably be as old as Late Permian and it could, locally, be as young as early Late Triassic (Carnian) based on young outliers in LA-ICPMS U-Pb detrital zircon age populations (Dickinson & Gehrels, 2009; Olsen et al., 2018; and Riggs et al., 2020). Riggs et al. (2020) presented an outcrop derived LA-ICPMS U-Pb detrital zircon age with a mean estimate of 250 ± 2 Ma for the Holbrook Member near Winslow Arizona, which would be earliest Triassic, with some zircon crystals reflecting a latest Permian age.

Although the Moenkopi Formation has a long history of paleomagnetic studies (Steiner et al., 1993; and references therein), previous work has relied heavily on the aforementioned biostratigraphic data for constraining any magnetostratigraphic correlations and was often limited by sampling short sections at coarse stratigraphic resolution. To help address these issues, this study concentrates on the high-resolution magnetic polarity stratigraphy of a continuous ~88- m-thick Moenkopi Formation section with unambiguous superposition and associated U-Pb age constraints, disconformably underlying the Upper Triassic Chinle Formation strata that the CPCP-1 cores intersected at PFNP, northeast Arizona, U.S.A. Despite the relatively thin total sequence of Moenkopi strata obtained in the CPCP-1 cores, our goal, given the opportunity for very high-resolution sampling, was to obtain a robust magnetic polarity stratigraphy for the entire section that can be correlated with previously reported polarity data from the formation elsewhere in Colorado Plateau area (e.g., Shoemaker et al., 1973; Steiner, 1986; Steiner et al., 1993; and Steiner & Lucas, 1992). This effort will also allow correlations with recent estimates of the global geomagnetic polarity timescale for the Early to Middle Triassic from marine sections (e.g., Hounslow & Muttoni, 2010; Li et al., 2018; Ogg, 2012; and Ogg et al., 2020), and more robust age estimates for the geographically proximal to outcrops producing important fossil assemblages.

2. Geologic Background: Early to Middle Triassic Depositional Setting

During the Pennsylvanian through Early Permian, parts of the central-western North American craton were involved in a diffuse intraplate deformation event that resulted in several NW–SE-trending Proterozoic-cored uplifts, often referred to as the Ancestral Rocky Mountains (ARM) with associated adjacent sedimentary depocenters (Brotherton et al., 2020; Kluth & Coney, 1983; and Soreghan et al., 2012). These highlands remained a source for detritus that was transported westward and southwestward into the Moenkopi and Chinle depocenters. An alternate or secondary source is the incipient Cordilleran arc, which provided an additional western-derived source for the Moenkopi Formation and its equivalents (Riggs et al., 2020). Regardless of the details of the tectonic settings and processes, most of the sediment of the Moenkopi depocenter was transported in west to northwest flowing fluvial systems, and the depositional environments varied, depending on location, from shallow marine to shoreline, to deltaic (Blakey, 2008; Olsen et al., 2018; and Riggs et al., 1996, 2020). Blakey (1973, 1974) concluded that most of the Moenkopi Formation west of the Colorado River is of marine, coastal, and proximal fluvial affinity and to the east, predominantly nonmarine (fluvial) with minor marine deposits. In southeast Utah, Moenkopi strata were deposited in a transitional environment. On the Colorado Plateau and its proximity, the overall depositional setting remained nonmarine to marginal marine through the entire early Mesozoic. These famous epicontinental basin deposits are rich in fossils and contain a climatic and tectonic record of west-equatorial Pangea and evolution of Triassic-Jurassic continental biota (Olsen et al., 2008, 2018).

Within the Little Colorado River drainage of northeastern Arizona, including Petrified Forest National Park, the Moenkopi Formation is interpreted as exclusively alluvial and fluvial (McKee, 1954), with the evidence
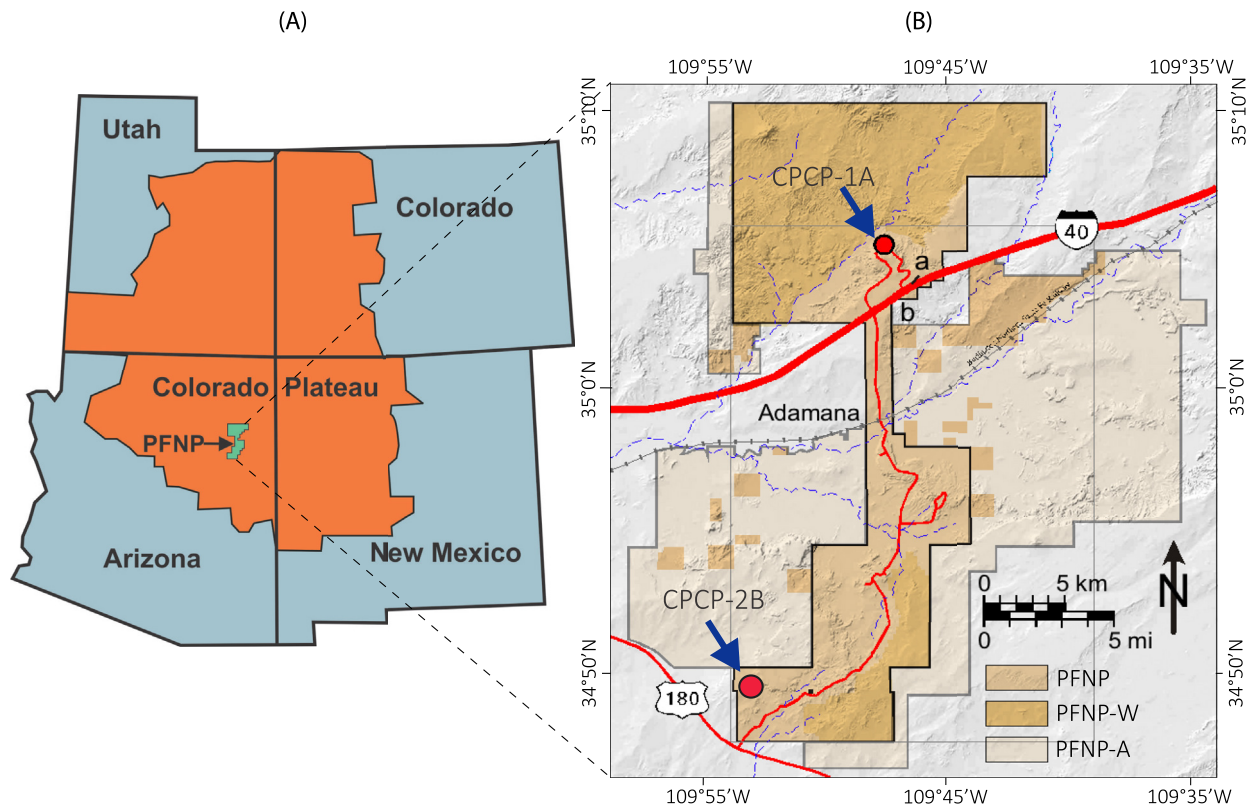
Figure 1. Location of the Colorado Plateau and the Petrified Forest National Park (PFNP) in northeast Arizona (a) and locations of the coring sites in the PFNP (b). Core CPCP-1A and core CPCP-2B collection sites are about 30 km apart. a—park headquarters; b—park entrance; PFNP-W—Wilderness area; and PFNP-A—Private or State Trust land (modified from Olsen et al., 2018).

of semiarid to arid origin for some of the gypsum-bearing units (Baldwin, 1973; and Stewart et al., 1972). In this region, the unit is divided into three conformable lithostratigraphic units from the oldest to the youngest: the Wupatki, Moqui, and Holbrook members. The central feature of this lithostratigraphic scheme is that the base of the Moqui Member is defined by the appearance of the first gypsum layer, whereas the top of the member is defined by the last gypsum layer (McKee, 1954; and Stewart et al., 1972). Also important is a regional marker bed named the "lower massive sandstone," which is a distinctive, thick, light-colored, cliff-forming sandstone near the top of the Wupatki Member that can be traced from the east of Holbrook, Arizona (i.e., the vicinity of PFNP) to the west of Lees Ferry near the Arizona-Utah border (e.g., McKee, 1954: Figures 4–6; and Stewart et al., 1972: pl. 3).

3. Coring and Paleomagnetic Sampling

Sampling of entire sections of Moenkopi as well as overlying Chinle strata as surface exposures has proven difficult because of the lack of continuous outcrop and/or surface-related chemical alteration, and the CPCP-1 drilling experiment allowed the acquisition of a continuous core of the Triassic section in unambiguous superposition (Olsen et al., 2018). The CPCP-1 drilling was conducted in Petrified Forest National Park (PFNP), northern Arizona (Figure 1), where Moenkopi and Chinle Formation strata are well represented (Heckert & Lucas, 2002; Martz & Parker, 2010; Martz et al., 2013; and Olsen et al., 2018; Parker, 2006), and have also been studied at nearby exposures (e.g., zircon U-Pb geochronology by Ramezani et al., 2011 and Riggs et al., 2003 and magnetic polarity stratigraphy by Steiner & Lucas, 2000; Steiner et al., 1993; and Zeigler et al., 2017). The rationale for obtaining cores from both parts of the PFNP was that this would allow the CPCP team to assess lateral variations in stratigraphy and the consistency of paleomagnetic polarity stratigraphy (Olsen et al., 2008, 2018). Because of the low latitudinal location of the Colorado Plateau during the Triassic Period, inclination alone cannot yield a magnetic polarity stratigraphy (Molina-Garza
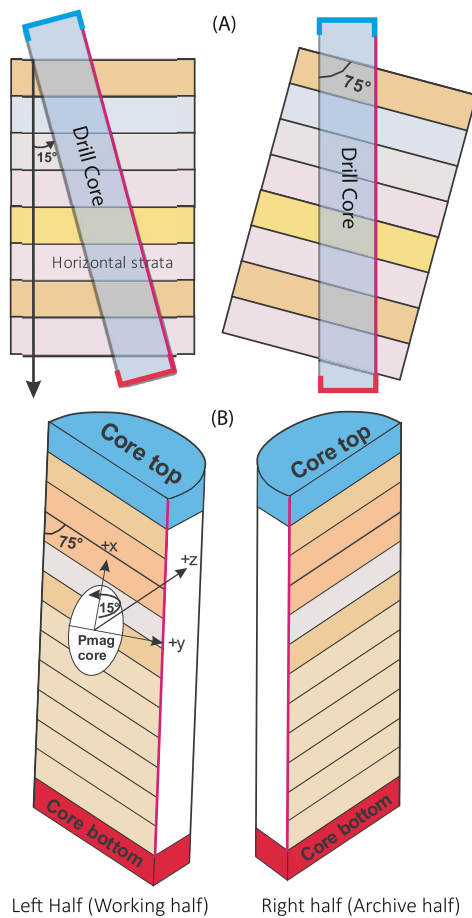
Figure 2. Schematic representation of coring (CPCP-2B) and subsequent paleomagnetic sampling orientations. (a) 2D- view of the core CPCP-2B that was drilled at 75° inclination into horizontal/sub-horizontal strata with an azimuth of 203°. (b) Cores were sliced into two halves along the azimuth marking and designated as working half (left-portion) and archive half (right-portion). Paleomagnetic samples were drilled perpendicular to the core face from the working half and rotated for 15° counterclockwise direction with the center of rotation along *z*-axis and then paleomagnetic axes were marked for measurements.

et al., 1991), and thus, core orientation was critical to have better control on remanence declination and several attempts were made to assure accurate core orientation. An inclined core penetrating flat-lying strata allows for approximate core orientation using the angular relationship between core edge and bedding or other physical proxies for bedding, and cores CPCP-1A and CPCP-2B were drilled at an azimuth/plunge of 135°/60° and 203°/75°, respectively. In addition, core azimuthal orientation (the uppermost edge of the core) was tracked using a REFLEX ACT II/III tool. At the LacCore Facility (University of Minnesota) cores were cut lengthwise into two equal halves along the REFLEX azimuthal marking; looking downhole the observer's left segment was designated as the working half and the right segment as the archive half. Although the cores remain the legal property of the National Park Service, the working half of each core is permanently stored at the Rutgers University core repository and the other halves are saved as archive material at the University of Minnesota. CPCP-1A is officially cataloged as PEFO 39602 and CPCP-2B as PEFO 39604, and permission is required from the Petrified Forest National Park to sample and research these cores.

Paleomagnetic cores were obtained by drilling perpendicular to the split face of the working half using a water-cooled diamond bit drill press assembly at the Rutgers University Core Repository, with an interval spacing ranging from a few centimeters to a decimeter in core CPCP-2B and half a meter to meter in core CPCP-1A. Each paleomagnetic core was cut into a standard 2.5 cm diameter and 2.25 cm high specimen for analyses. Given the dimensions of the split core, only one standard specimen could be suitably prepared from each drilled core sample. Counterclockwise rotations of 30° and 15° were made before marking the +x, +y, and +z directions on the paleomagnetic specimens to account for the plunge of the cores CPCP- 1A and 2B, respectively, and therefore, we use an azimuth/hade of 135°/90° (CPCP-1A) and 113°/90° (CPCP-2B) to restore the cores into their geographic coordinates (Figure 2). The details of the entire CPCP-1 drilling experiment and further details regarding core orientation and processing can be found in Olsen et al. (2018).

4. Laboratory Methods

A total of about 540 oriented specimens were obtained from the core interval of ~140–230 m core depth (mcd), which is ~135–222 m stratigraphic depth (msd), from the CPCP-2B core. We also reanalyzed the data from about 110 specimens studied by Buhedma (2017) in his unpublished MS thesis, which covers the CPCP-1A core interval of ~410–511 m, mcd (~355–442.5 m, msd), and we obtained additional samples from selected intervals of core CPCP-1A. In addition, for core CPCP-2B, we routinely drilled several samples from individual, intact drill core segments, to test for the internal consistency of paleomagnetic data. Several paleomagnetic and rock magnetic analyses were conducted to identify the magnetic polarity and the mineralogy of these rocks.

Progressive thermal demagnetization (PTD) was used to isolate the components of the natural remanent magnetization (NRM). Specimens were heated in ASC TD-48 furnaces stored in a magnetically shielded room with a peak magnetic field of less than 10 nT. The NRM and remanence after all demagnetization steps were measured using either a 2G-Enterprises cryogenic magnetometer equipped with DC-squids or AGICO JR6A spinner magnetometers housed in a magnetically shielded room. Orthogonal vector (Zijderveld, 1967) diagrams were used to plot the remanence directions at each PTD step. Magnetization directions were obtained by a least squares best-fit line constructed over several (usually 7–12 steps) PTD steps following the principal component analysis approach of Kirschvink (1980), using the AGICO software

Remasoft. Demagnetization data were typically anchored to the origin because most specimens exhibited a well-defined stable endpoint demagnetization behavior showing a trend directly to the origin. PTD steps typically in the range of ~275–680°C were used to assess the characteristic remanent magnetization (ChRM) directions and individual specimen directions were accepted if the maximum angular deviation (MAD) of best-fit, anchored to the origin, line values were <15°. Isothermal remanent magnetization (IRM) acquisition and backfield demagnetization of saturation IRM (SIRM) experiments were conducted with an ASC Scientific multi-coil impulse magnet. Three component thermal demagnetization of IRM (Lowrie, 1990), acquired in peak fields of 2.97 T, 1.2 T, and 0.3 T, in that order, were performed to understand the magnetic mineralogy and measurements were made using AGICO JR6A spinner magnetometer. Thermomagnetic analysis of crushed specimens was conducted to monitor any mineralogic alteration and identify the principal magnetic mineralogy. An AGICO MFK1-A susceptibility instrument interfaced with a CS4 high-temperature furnace was used for heating-cooling susceptibility measurements, which were conducted both in air and in an inert atmosphere. Anisotropy of magnetic susceptibility (AMS) measurements were obtained on all specimens of appropriate size/shape from the core CPCP-2B to identify the depositional and if any post-depositional fabrics present. An AGICO MFKI-A system equipped with an automatic 3D-rotator (Studýnka et al., 2014) was used for AMS measurements. Fifteen petrographic 30 μm standard thin sections were made from core samples of selected intervals of the Moenkopi Formation from the core CPCP-2B for petrographic and scanning electron microscopy (SEM) inspection.

U-Pb detrital zircon ages from Gehrels et al. (2020) and Rasmussen et al. (2020) are here represented as relative probability density plots (Figure 12). This approach is particularly useful for these Moenkopi data for several reasons. First, it allows an accurate representation of samples with complex age inventories, where picking a coherent age population to calculate a weighted mean age, and hence a maximum depositional age is not straight forward (e.g., Rasmussen et al., 2020: sample 319Y-2 in Figure 2). Second, it is the only way to directly compare the age distributions where samples comprise both CA-TIMS and LA-ICPMS ages; multiple studies demonstrate that the application of these methods to the same crystals often results in individual crystal and weighted mean ages that do not overlap in uncertainty (e.g., Herriott et al., 2019; Rasmussen et al., 2020; and von Quadt et al., 2014). Finally, for LA-ICPMS age estimates, where larger analytical uncertainties can often mask separate, but closely spaced age populations, relative probability density plots provide more uncertain, but more accurate representations of the distribution of possible ages for a sample.

5. Results

### 5.1. Magnetic Mineralogy and Magnetic Fabrics

Several studies have shown that the characteristic remanent magnetization (ChRM) in red sedimentary rocks is largely carried by specularite grains of detrital origin, rather than by the microcrystalline hematite pigment, as can be partly demonstrated using progressive chemical demagnetization (e.g., Collinson, 1975; Tauxe et al., 1980). Petrographic inspection of the selected Moenkopi samples in this study confirms the presence of abundant hematite as opaque detrital grains as well as very fine translucent authigenic coatings on detrital silicate grains (Figure 3). Scanning Electron Microscopy/Energy Dispersive X-Ray Spectroscopy (SEM/EDS) analysis on the representative specimens also confirms the presence of rounded to subrounded specularite (iron-titanium oxides) and fine, euhedral (platelets), authigenic likely of hematite grains (Figure 4). Several rock magnetic analyses including the isothermal remanent magnetization (IRM) and backfield demagnetization of saturation IRM, three component thermal demagnetization of IRM, and unmix analysis of the IRM acquisition data confirm that the dominant magnetic carriers in the Moenkopi rocks is hematite with a minor presence of magnetite/titanomagnetite and maghemite (Figures S1–S3). Thermomagnetic analysis of magnetic susceptibility was carried on powdered specimens from all three members of the Moenkopi Formation rocks. Thermomagnetic curves show a gradual decrease in susceptibility with two steeps drop at ~600°C and 680°C, which suggests the presence of magnetite and hematite. Bulk susceptibility curves during continuous heating and cooling (χ-T) usually show an overall increase in susceptibility as a result of the heating experiment, thus revealing some degree of magnetic mineral alteration during thermal treatment. Both in the presence of air and inert conditions, all specimens yield essentially reversible heating and cooling curves from about 560° to 680°C, suggesting no substantial hematite mineral alteration during these experiments, and irreversible curves up to ~560°C, suggesting the formation of minor magnetite
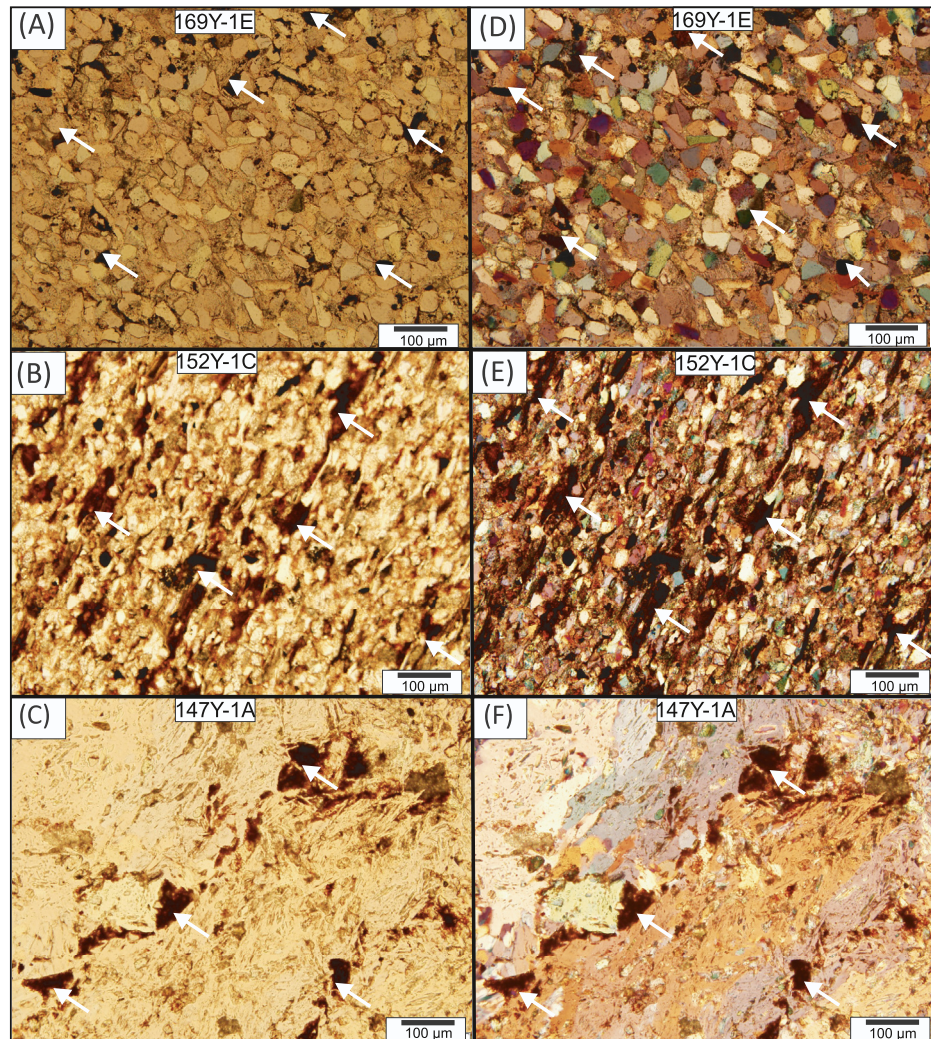
Figure 3. Representative photomicrographs from the Moenkopi Formation rocks showing the presence of hematite in the matrix as detrital grains (white arrows) and authigenic coatings. Observations under transmitted plane-polarized (a–c) and transmitted cross-polarized light (d–f).

during heating (Figure 5). Overall, reversible χ-T curves in a reheated experiment indicate no thermal alteration during the re-experiment of the same specimens. Few specimens yield sharp single-domain-type Hopkinson peaks at 580°–620°C, indicating a transition from stable magnetization to a superparamagnetic phase.

AMS fabrics of detrital sedimentary rocks or unconsolidated detritus may depict a preferred orientation of the magnetic (paramagnetic and ferrimagnetic) minerals and hence, can provide critical information on the primary, depositional, and subsequent deformation fabrics of detrital sedimentary rocks (Haque et al., 2020; Hrouda, 1982; Parés, 2015; Tarling & Hrouda, 1993). AMS data from CPCP-2B specimens, separated by Moenkopi lithostratigraphic member, all show a well-grouped, vertical/sub-vertical minimum susceptibility axis and dispersed maximum and intermediate axes about the perimeter, and this girdle pattern is typical of fine-grained detrital sedimentary rocks with a well-preserved depositional fabric (Haque et al., 2018, 2019; Hrouda, 1982; Tarling & Hrouda, 1993) (Figure 6). The shape parameter versus the degree of anisotropy plots show a predominantly oblate (disc) shape suggesting a fine-grained, low-energy depositional environment. The overall low-bulk susceptibility (50–300×10^{-6} SI volume) indicates the absence of an appreciable concentration of magnetite/titanomagnetite grains, consistent with other rock magnetic observations. Notably, the members of the Moenkopi Formation yield distinguishing magnetic susceptibility
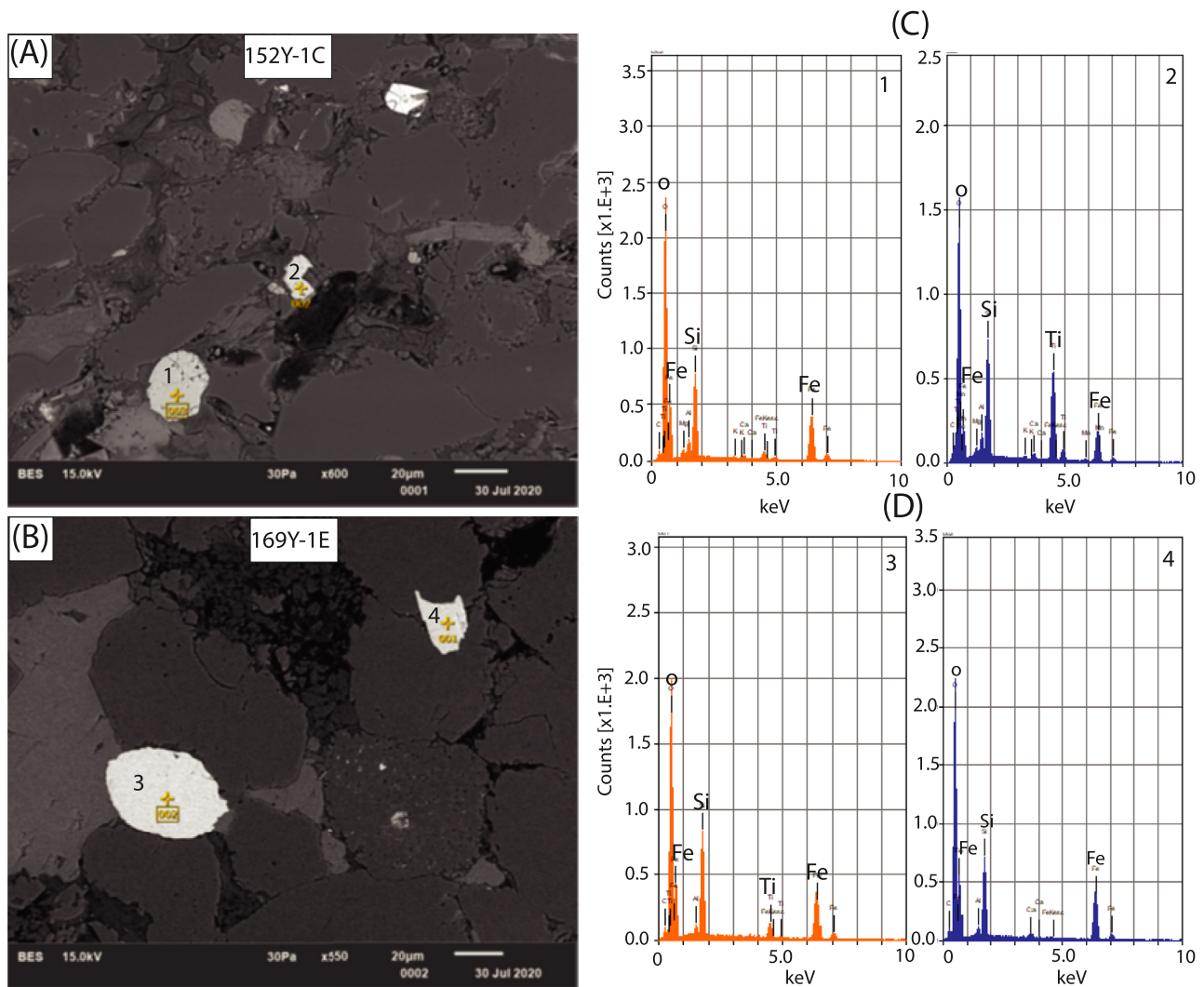
Figure 4. Scanning electron microscopy (SEM) backscattered electron image (a–b) and Energy Dispersive X-Ray Spectroscopy (EDS) (c–d) analysis on representative specimens. The SEM images showing the presence of both rounded to subrounded detrital and euhedral authigenic iron-oxide grains. Due to the higher atomic number, iron-titanium oxide grains are bright compared to the surrounding grains. The uniform brightness suggests uniform atomic distribution. EDS shows the relative abundance of elements with the peaks at Fe (iron), O (oxygen), Ti (titanium), and Si (silicon). A constant silicon abundance in all EDS analysis including in the iron-titanium oxides indicates that the silicon peaks are mostly from the background materials.

results. For example, specimens from the Holbrook Member have the highest median bulk susceptibility and show a very uniform, low degree of anisotropy as well as the relatively lowest shape parameter value. The Wupatki Member, on the other hand, has the lowest degree of anisotropy and intermediate median bulk susceptibility and highest shape parameter values among the members of the Moenkopi Formation (Figure 7).

### 5.2. Characteristic Remanent Magnetization and Magnetic Polarity Zonation

Specimens prepared from the Moenkopi Formation from cores CPCP-1A and CPCP-2B typically yield high quality and interpretable demagnetization results as has been reported for outcrop studies of this formation (e.g., Haque et al., 2018, 2019; Steiner et al., 1993, and references therein). The natural remanent magnetization (NRM) intensity of most specimens from the CPCP cores ranges from 2 to 20 mA/m. Laboratory unblocking temperature spectra show a gradual decrease in magnetization up to about 650°C, and then a relatively rapid decrease over a narrow temperature interval from about 660°C to about 682°C (Figure 8). Well over 90 percent of the specimens provide an interpretable demagnetization response with a maximum
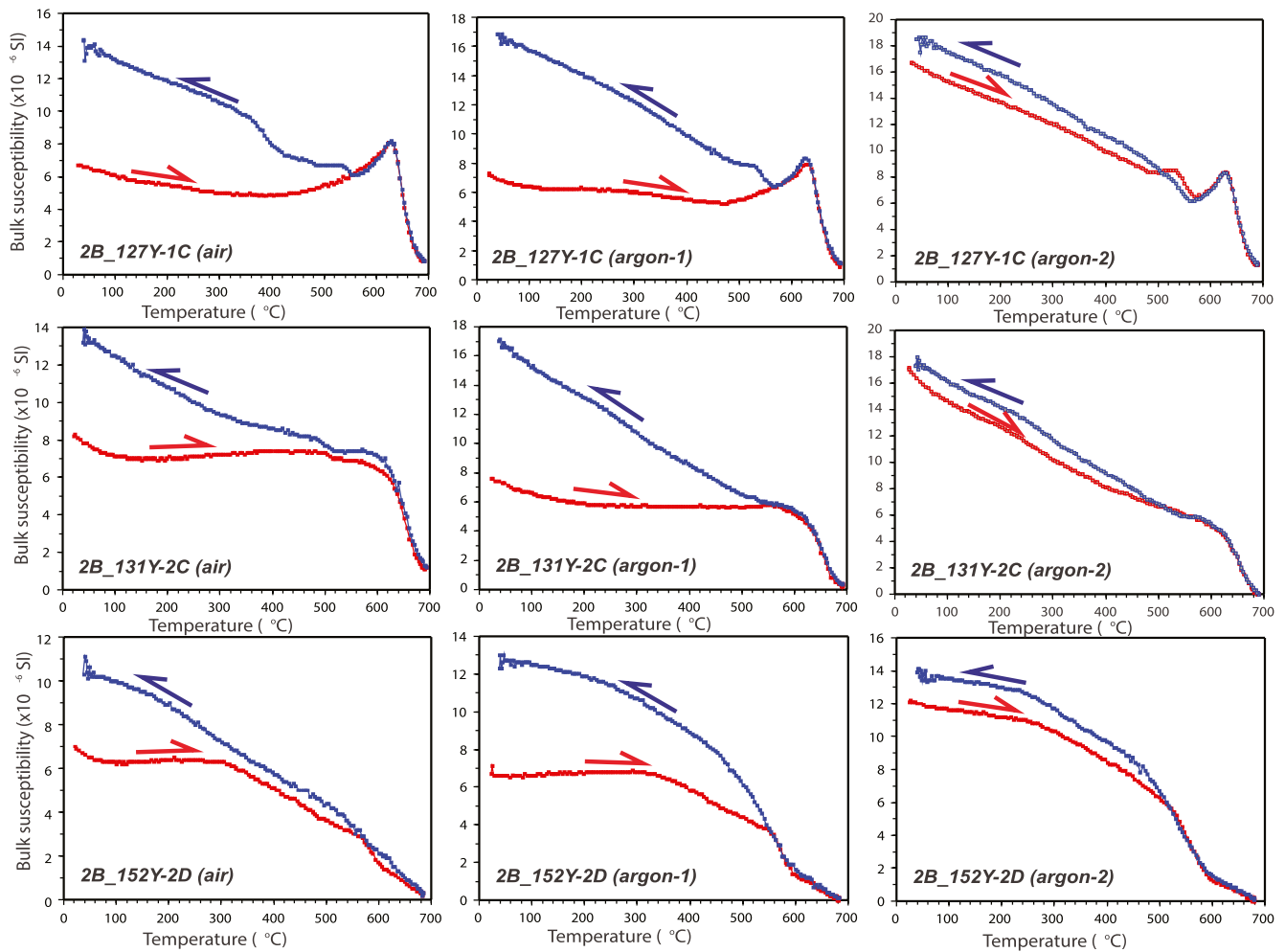
Figure 5. Temperature dependence of magnetic susceptibility curves (heating and cooling cycles) of powdered specimens from different stratigraphic levels of the CPCP-2B core. The red and blue lines indicate heating and cooling curves, respectively.

angular deviation (MAD) value, using anchored line segments, determined using at least 7–12 demagnetization steps, of well less than 15° (Figures 9 and 10). The NRM of specimens typically consists of two components and the Zijderveld (1967) vector endpoint demagnetization diagrams show that progressive thermal demagnetization suitably unblocks a relatively low laboratory unblocking temperature component in the range of ~250°–495°C, which is inconsistent in orientation, followed by a magnetization component that is unblocked over a relatively distributed and then more discrete range of high temperatures up to ~682°C in most specimens. It is this high-temperature component that we interpreted as the characteristic remanent magnetization (ChRM). Only a few specimens, mostly in the Holbrook Member, show a secondary component that unblocks at high temperature above 500°C (Tables S1–S4). At face value, without any consideration of possible core segment misorientation (rotation or flipping) and adjustment, most ChRM directions cluster about NNW/SSE declinations and shallow inclinations (Figures 9 and 10). The two populations of directions, one north-seeking and shallow, dominated by positive inclination, and the other south-seeking and shallow, with some negative inclination values, are interpreted as normal and reverse polarity Triassic geomagnetic field directions, respectively.

However, a small number of results from specific, intact core segments are characterized by internally consistent ChRM directions, yet all specimens from these segments yield declinations that deviate considerably with respect to either the NNW- or SSE-directed populations of results, suggesting a strong likelihood of core rotation during either drilling or core extraction. For such unanticipated results, we used the physical bedding/core-edge relations (where possible) to attempt to correct for core misorientation and correctly
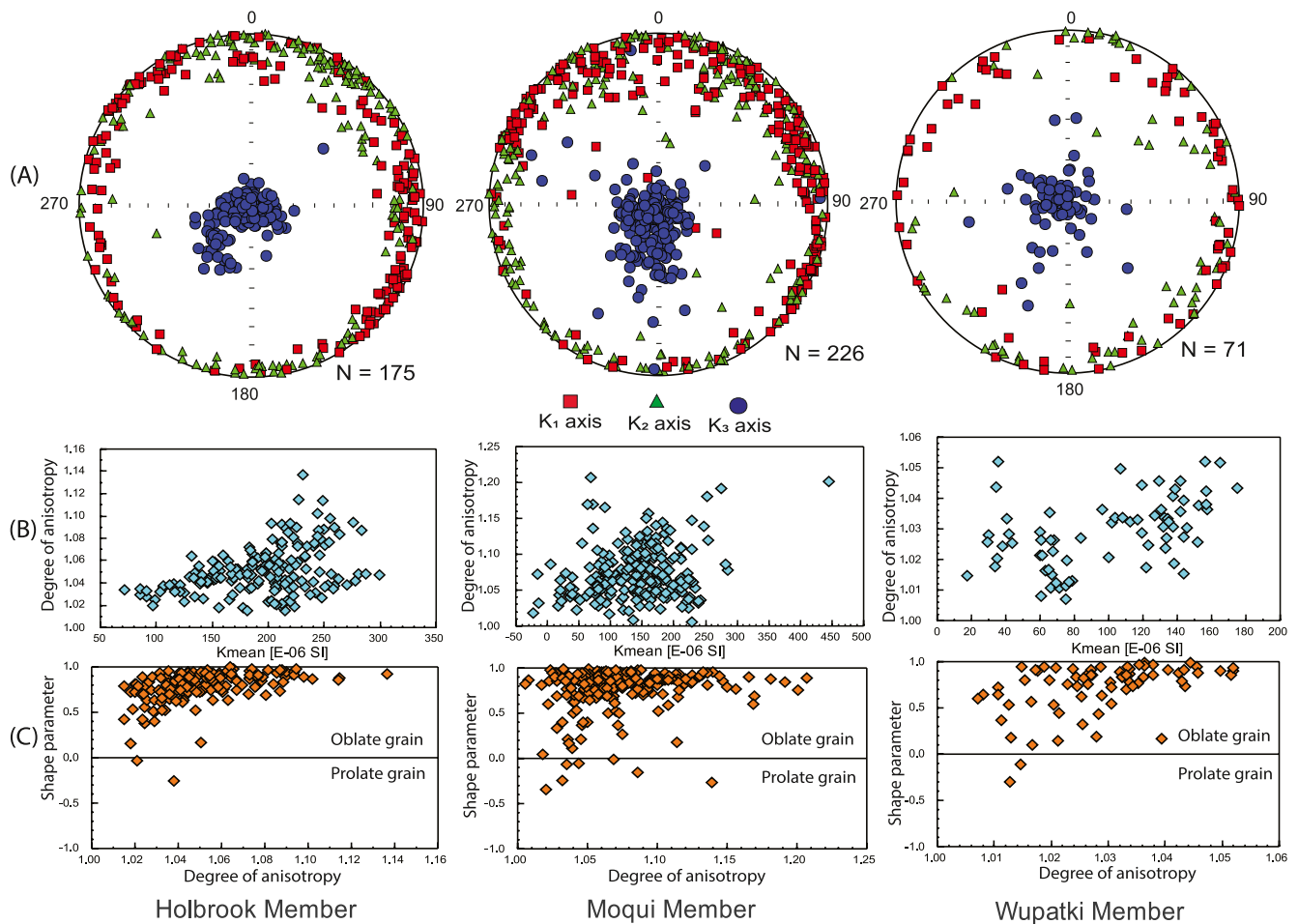
Figure 6. Anisotropy of magnetic susceptibility (AMS) data from the three lithostratigraphic members of the Moenkopi Formation intersected in the CPCP-2B core (a) Stereographic projections showing the directions of maximum, intermediate, and minimum susceptibility axes projected onto the lower hemisphere (b) bulk susceptibility versus degree of anisotropy (c) degree of anisotropy versus shape parameter.

interpret the polarity results. For an accurately oriented core segment, as discussed above, assuming that bedding/internal stratification, as a proxy for bedding in Moenkopi rocks, is essentially horizontal, these sedimentary features should be inclined to the left, from the right at about 60° and 75° in core CPCP-1A and CPCP-2B, respectively, in the working half and core edge/bedding relation is opposite in the archive half of the core (Figure 2). Rotation of the core segment during or after drilling modifies the physical bedding/core-edge relations. A rotation of 180° of the core segment, for example, will result in the core-edge/bedding plane relation being opposite from the correct orientation. A rotation of about 90° would result in the trace of bedding to be essentially perpendicular to the core-edge, and a rotation of less than 90° would yield a bedding/core-edge relation at some apparent angle. In addition, an intermediate magnitude of core segment rotation about the core axis, given the plunge of the CPCP-1A and CPCP-2B cores, would result in an inclination that is artificially steeper, in either a positive or negative inclination sense.

To overcome the possibility of core rotation affecting the distribution of paleomagnetic directions, several approaches were utilized to interpret the magnetic polarity record of the entire section obtained in core CPCP-2B. First, we only selected groups of specimens ("category-1") for polarity interpretation that yielded magnetizations consistent with expected geomagnetic field directions of Early to Middle Triassic age in the study area and exhibited the appropriate/predicted bedding/core edge relations. The expected declination calculated from the Torsvik et al. (2012) pole compilation for northern Arizona for the core CPCP- 2B site is 331.5° for 250 Ma and 334.7° for 240 Ma; in addition, it is 343.2° for the 230 Ma pole from the Kent and Irving (2010) compilation (Figure 10). To address the core rotation issue, we arbitrarily choose a range
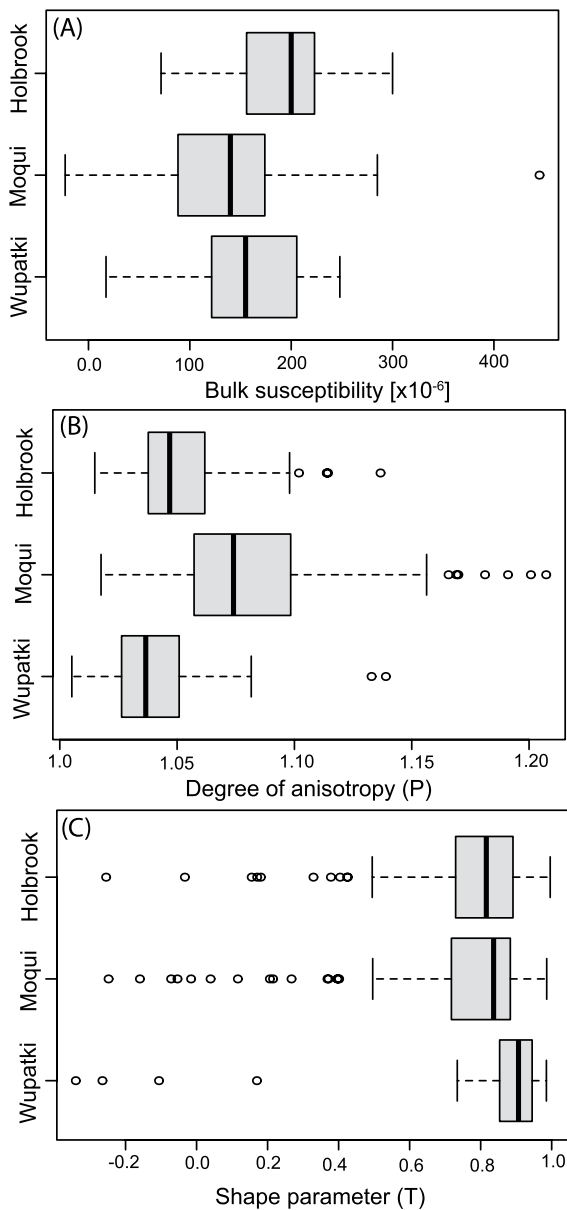
Figure 7. Boxplots showing the minimum, lower quartile, median, upper quartile, and maximum value of the bulk susceptibility (a), degree of anisotropy (b), and shape parameter (c) of the Moenkopi Formation rocks by members encountered in the CPCP-2B core. Boxplots suggest that each of the Moenkopi members has a distinguishing AMS (anisotropy of magnetic susceptibility) parameter/fabric.

of declinations from 300° to 10° (and the antipodal spread) from core segments with the appropriate bedding/core edge relations. About 65 percent ($n = 303$) of the accepted specimens providing interpretable demagnetization results fall into the "category-1" and thus yield directions within the range selected for polarity interpretation, with two sets of data (north and south directed) interpreted as of normal and reverse polarity, respectively. The mean ChRM direction for the "category-1" specimens, with reverse polarity data inverted through the origin, is Dec = 333.6°, Inc = +1.8°, $\alpha_{95} = 2.5°$, and $k = 11.54$ ($n = 303$). Second, if an entire group of specimens collected from a single core segment yielded internally consistent but deviatory declinations, yet displayed a somewhat appropriate bedding/core-edge relation ("category-2"), we considered these core segments to have been rotated, but not significantly enough to produce opposite bedding/core-edge relations, and we interpreted their polarity based on the nearest expected field direction. About 18 percent ($n = 85$) of the interpreted specimens fall into this category. A small number (one/two) of specimens in a few multi-sampled core segments, which shows correct bedding/core-edge relations, yield deviating declination results, and the other specimens from the same core segment yield directions that are consistent with an Early to Middle Triassic field. We considered that these results were likely misoriented during subsequent paleomagnetic sampling and processing, although we have marked the core face before drilling to avoid such misorientation. Specimens that produced unusually high-inclination values are also considered under this category. Only a few of the interpreted specimens (~5 percent, $n = 23$) fall in this category, and they do not affect the overall magnetic polarity zonations. Fourth, for those specimens that produced interpretable demagnetization results but ChRM declinations that deviated by over 30° degrees from either normal or reverse polarity declination distributions and were from core segments that clearly show opposite bedding/core-edge relations ("category-4"), we attempted to reorient the core to an appropriate configuration using a planar sedimentary feature (e.g., bedding); yet in a few cases, we simply disregarded these data for polarity interpretation. About 12 percent of the specimens ($n = 48$) fall in this category. Overall, core rotation appears to be less of a significant factor for core CPCP-1A, with about 80 percent of the analyzed specimens of "category-1," yielding declinations consistent with expected field directions of Early to Middle Triassic age with a mean direction of Dec = 340.8°, Inc = −1.1°, $\alpha_{95} = 5.5°$, and $k = 8.4$ ($n = 90$).

To interpret the magnetic polarity record of the entire Moenkopi section, we used an approach essentially as described in Kent et al. (2018, 2019). The ChRM direction for each accepted specimen was converted to a virtual geomagnetic pole (VGP) whose latitude was rotated with respect to the 230 Ma reference (north) pole (Kent & Irving, 2010), and referred to as rVGP latitude (toward +90° for normal and −90° for reverse polarity). At least two and usually many more consecutive samples with the same polarity were used for interpreting polarity zones (magnetozones) from core CPCP-2B and because of a lower sampling density, one or more consecutive samples with the same polarity were used for interpreting magnetozones from core CPCP-1A. We correlated the polarity intervals generated from the "category-1" specimens and those polarity intervals generated from both ("category-1 and 2") specimens and a good agreement of the polarity zonation from both categories of specimens suggest that, due to our relatively high sampling density and the absence of appreciably thick intervals where a continuous core misorientation occurred, there is most likely no appreciable gap in the polarity zonation obtained from core CPCP-2B.
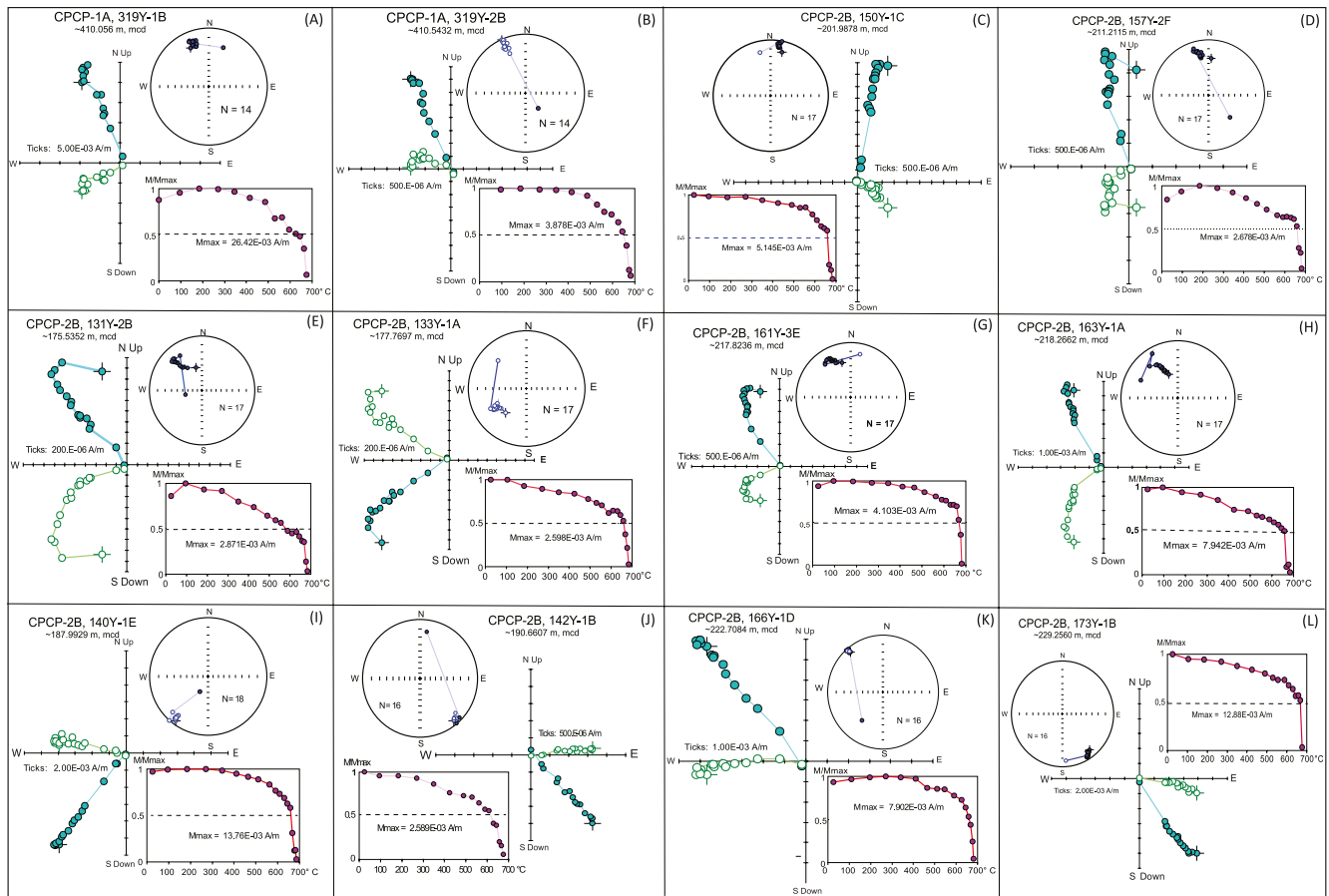
Figure 8. Examples of progressive thermal demagnetization results for representative samples from cores CPCP-1A and CPCP-2B. Equal area projection of magnetization vector showing the magnetization direction at each demagnetization step (solid and empty circles represent lower and upper hemisphere projection; respectively) in geographic coordinate and normalized intensity decay plots showing the response to thermal treatment. mcd, meters core depth.

Compilations of rVGP latitudes with depth for Moenkopi sections show considerable similarity in terms of magnetozones identified in both cores CPCP-1A and CPCP-2B, regardless of the relatively lower sampling frequency in the CPCP-1A core. Because of the relatively high-sampling frequency for the CPCP-2B core, and the fact that data from CPCP-1A are not incompatible with CPCP-2B, we accept the polarity stratigraphy of CPCP-2B as representative of the section. We assume that the observed slight differences in thicknesses of magnetozones between CPCP-1A and CPCP-2B cores are mostly due to a lateral variation in local sediment accumulation rate and differences in sampling density (Figure 11). The consistency of the polarity zonations between the two cores, coupled with the overall high sampling density for the CPCP-2B core, are interpreted to indicate that this study has identified all of the magnetozone intervals captured by the Moenkopi Formation characteristic of this area of the Colorado Plateau. The Moenkopi Formation in the study area contains 12 magnetozones, which we have designated as MF1n to MF6r from stratigraphically highest to lowest, extending from the uppermost Holbrook Member, which is disconformably overlain by the Mesa Redondo Member of the Chinle Formation, to the Wupatki Member of the Moenkopi Formation, which is disconformably underlain by the Upper Permian Coconino Sandstone.

The expected inclination calculated from the Torsvik et al. (2012) pole compilation for North America for the Moenkopi Formation in northern Arizona is ±24° (±18°) for 250 Ma (240 Ma) and ±13.0° based on the 230 Ma pole from the Kent and Irving (2010) compilation. Due to the equatorial paleo-latitudinal position of the Colorado Plateau during the deposition of the Moenkopi strata, a mixture of positive and negative inclinations is observed from a single polarity population; and in such a case, the mean inclination may be biased toward a shallower inclination (McFadden & Reid, 1982). The calculated mean inclination following
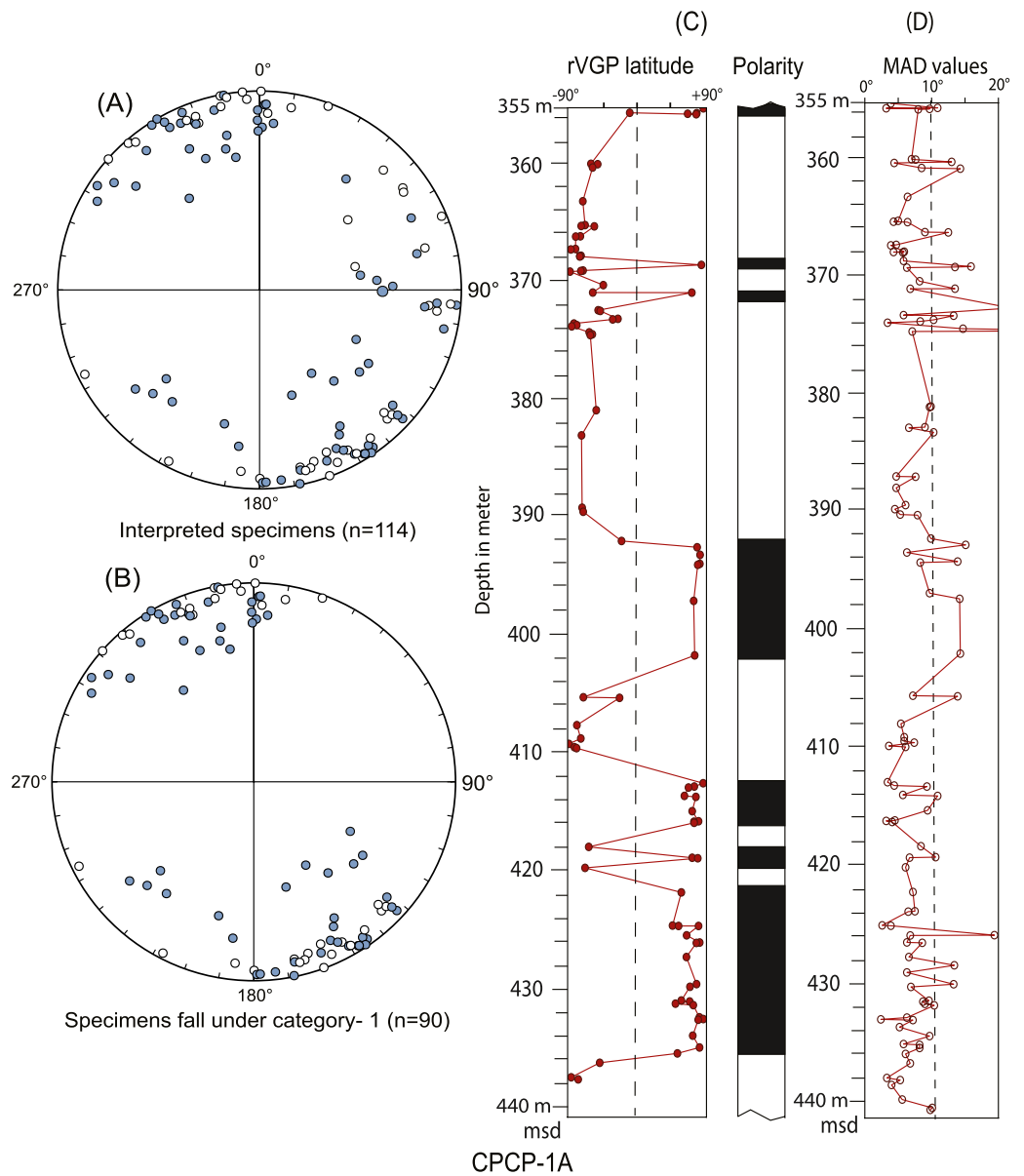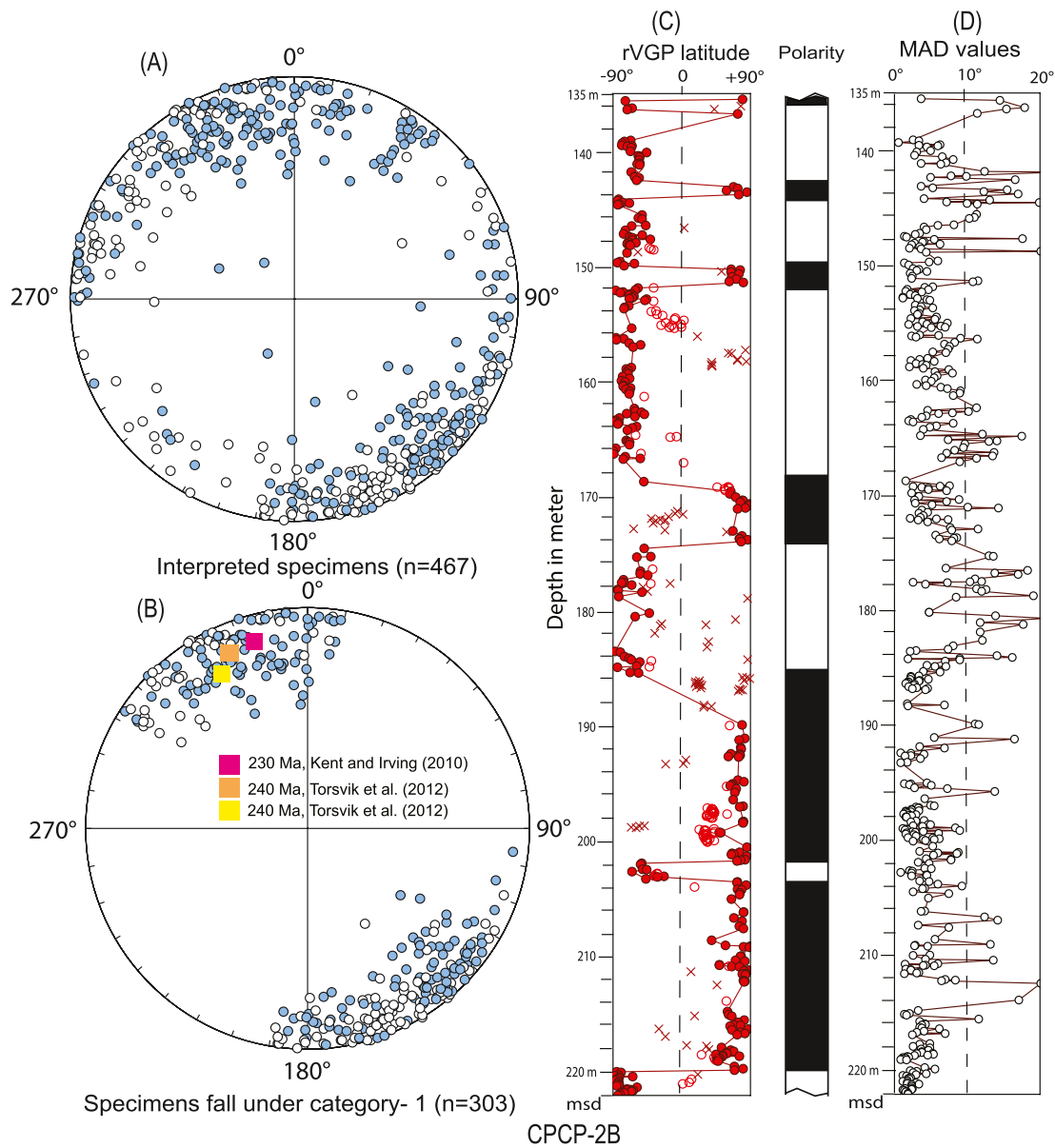
Figure 9. Equal area projection of the characteristic remanence magnetization (ChRMs) of specimens from the core CPCP-1A and their associated interpreted magnetozones. (a) ChRMs from all the interpreted specimens, (b) ChRMs of the specimens obtained from the core segments that have acceptable bedding/core-edge orientations (category-1), (c) rotated virtual geomagnetic pole (rVGP) latitude of the acceptable specimens and interpreted magnetozones and (d) maximum angular deviation (MAD) values of all the interpreted specimens.

the Arason-Levi inclination-only method (Arason & Levi, 2010), yields a mean inclination of +4.86°, with the precision parameter (k) of 12.66 and a 95% confidence limit (α95) of 1.92° (n = 461).

6. Discussion

6.1. Magnetostratigraphy

Generally, red beds are more strongly magnetized than other sedimentary rock types and thus have been extensively used in paleomagnetic studies despite the controversy over their timing of remanence acquisition (Butler, 1982, and references therein; Kodama, 2012; and Walker et al., 1981). Surface exposures of the Moenkopi Formation have been extensively studied for paleomagnetic and magnetostratigraphic records

Figure 10. Equal area projections of the characteristic remanence magnetization (ChRMs) of specimens from the core CPCP-2B and their associated interpreted magnetozones. (a) ChRMs from all specimens yielding interpretable demagnetization results, (b) ChRMs of the specimens obtained from the core segments that have acceptable bedding/core-edge orientations (designated category-1) along with the expected Early to Middle Triassic paleomagnetic directions at CPCP-2B core site (squares), (c) rotated virtual geomagnetic pole (rVGP) latitude of the acceptable specimens and interpreted magnetozones, red solid, and open circles represent the rVGP latitude of category-1 and -2 specimens, respectively; and red-x symbols show those specimens that were disregarded from polarity interpretation, and (d) MAD (maximum angular deviation) values for all interpreted specimens.

(e.g., Steiner et al., 1993, and references therein). Previous studies on surface exposures of Moenkopi Formation strata indicate that hematite is the primary magnetic phase that contributes to the remanence in these rocks and that much of the hematite is authigenic in origin with minor detrital grains in the form of both ilmenite-hematite intergrowths (tiger-striped grains) and specular hematite (specularite) (Elston & Purucker, 1979; Walker et al., 1981). Studies have concluded that the acquisition of a characteristic remanent magnetization (ChRM) in Moenkopi strata was penecontemporaneous with deposition, perhaps within a few hundred years and thus that the formation did provide high fidelity magnetic polarity information for parts of, presumably, the Early to Middle Triassic (e.g., Liebes & Shive, 1982). Steiner et al. (1993) in their study of Moenkopi exposures in northern Arizona argued that, due to partial inaccessibility and/or
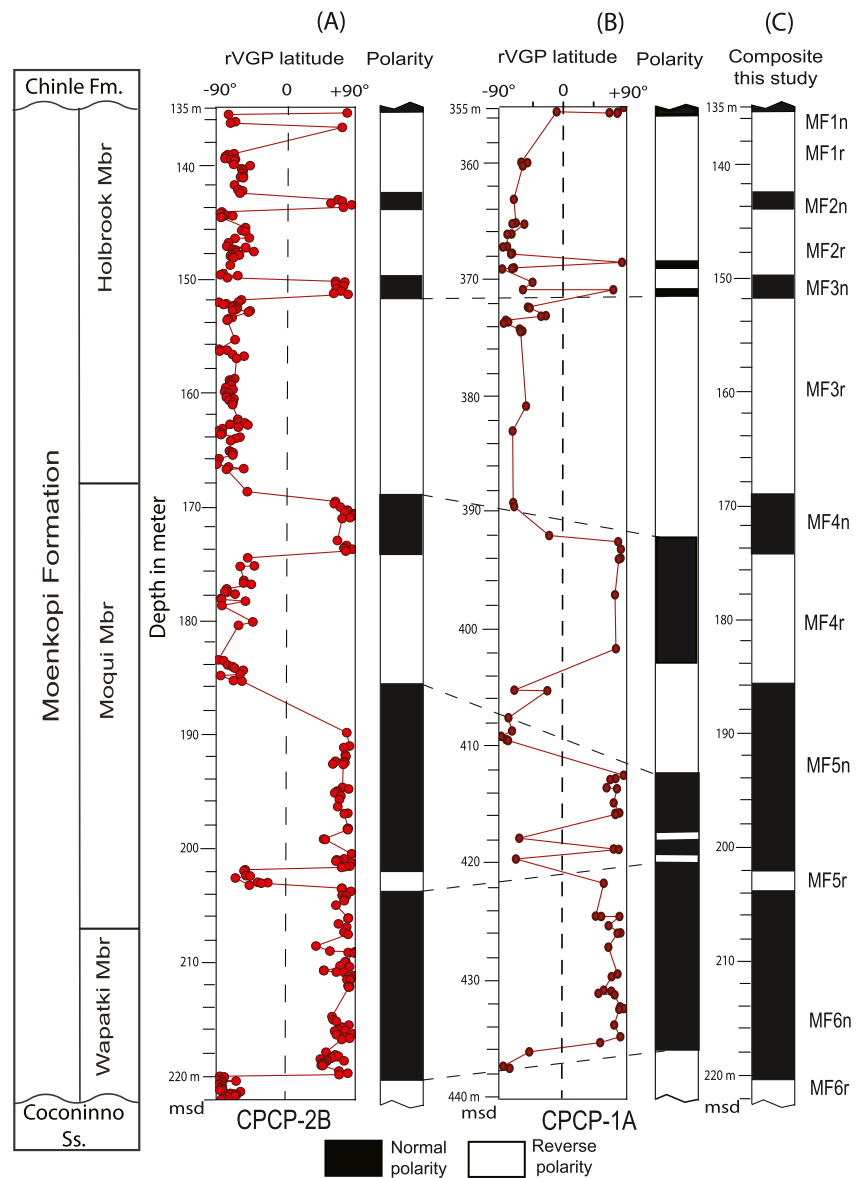
Figure 11. Correlation of the magnetic polarity zones obtained from cores CPCP-1A (a) and CPCP-2B (b). Magnetic polarity zones from both cores show a considerable similarity, regardless of their sampling frequency, and due to the higher sampling frequency in the CPCP-2B core, the polarity zonation of this core was used in the construction of inferred magnetic polarity stratigraphy of CPCP-1 cores (c).

geochemical alteration, the Moenkopi sections they sampled likely provide an incomplete magnetic polarity record. More recent compilations for the entire Triassic Period (Hounslow & Muttoni, 2010; Ogg, 2012; and Ogg et al., 2020) utilize a more global base of magnetostratigraphic data, with the recent reports on data from specific sections utilizing robust, modern approaches to develop magnetic polarity records, and where possible, specific numerical age information for parts of the Triassic. Finally, longer magnetostratigraphic records for the Triassic Period with cyclostratigraphic and marine biostratigraphic age control are also now available (e.g., Li et al., 2018).

In the Hounslow and Muttoni (2010), Ogg (2012), and Ogg et al. (2020) polarity timescales, the Early (Induan/Olenekian stages) and Middle (Anisian/Ladinian stages) Triassic includes a number of inferred polarity chron couplets, where Hounslow and Muttoni (2010) numbered the Early Triassic chrons as LT1 through LT9 and the Middle Triassic chrons as MT1 through MT13. With this as background information, the key
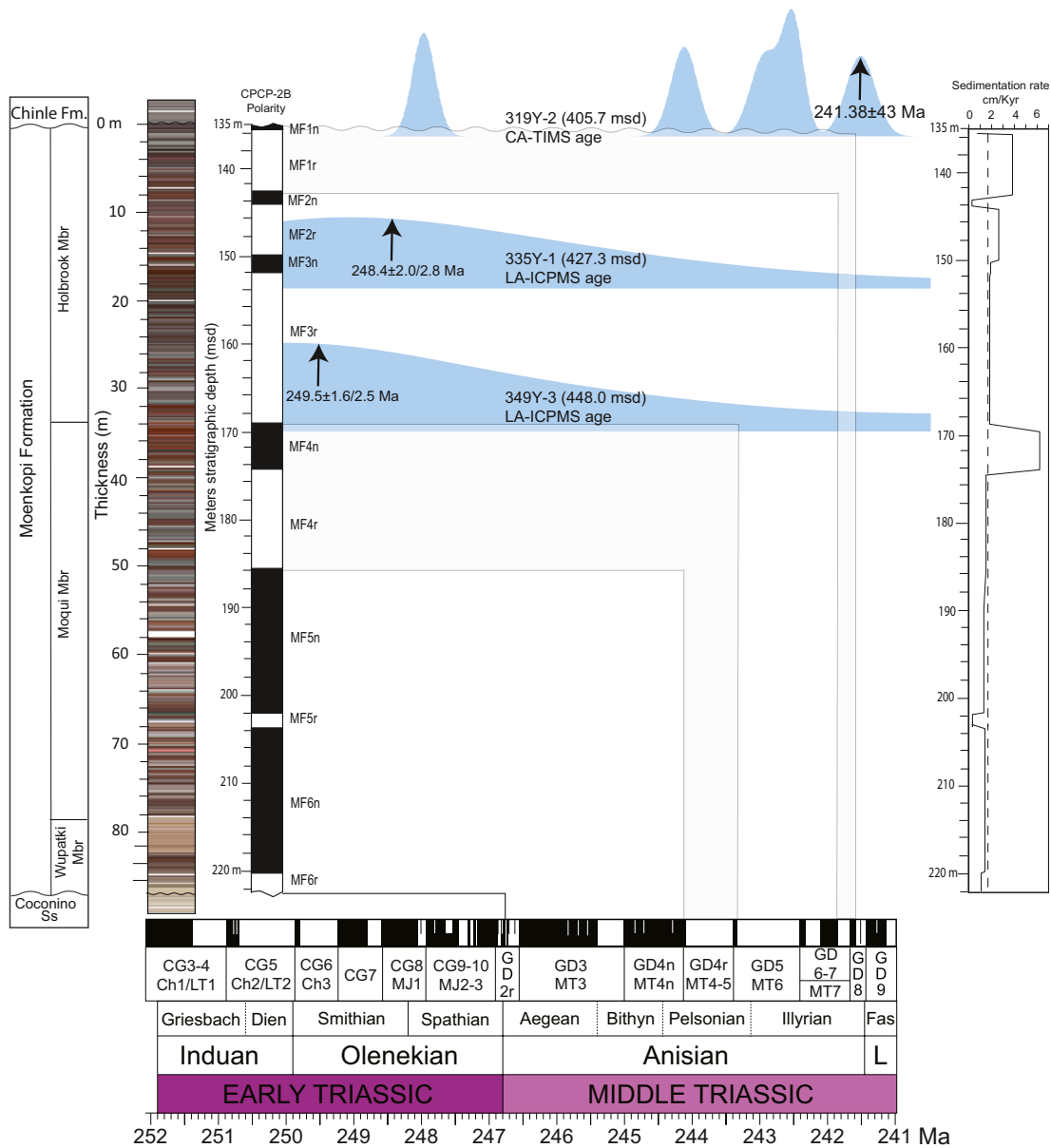
Figure 12. Correlation of the magnetic polarity stratigraphy from core CPCP-2B to the astronomically tuned (405 Kyr cycle) Early-Middle Triassic magnetostratigraphic timescale from Li et al. (2018, their Figure 9), which incorporates magnetic polarity patterns and nomenclature for the Early Triassic from the Szurlies (2007), and Hounslow and Muttoni (2010) proposed geomagnetic polarity time scales; and for the Anisian (Middle Triassic) from the Lehrmann et al. (2015), and Hounslow and Muttoni (2010) proposed polarity time scales. Blue represents the relative probability distribution curves of the CA-TIMS (chemical abrasion–isotope dilution–thermal ionization mass spectrometry) (Gehrels et al., 2020) and LA-ICPMS (laser ablation–inductively coupled plasma mass spectrometry) (Rasmussen et al., 2020) U-Pb dates from zircon populations of samples from equivalent stratigraphic positions in core CPCP-1A (see Figure S4 for full age distribution curves). Lithostratigraphic column shows the color profile from the spectrophotometer for that part of the core CPCP-2B. The rightmost column shows the average sedimentation rate calculated for each of the polarity chrons (solid line) and for the total Moenkopi Formation (dashed line) in centimeter per thousand years. Abbreviations: Bithyn—Bithynian; Dien—Dienerian; Fas—Fassanian; and Griesbach—Griesbachian.

question becomes whether the Moenkopi record can be reliably correlated with these recent estimates of the Triassic geomagnetic polarity timescale and, consequently, can we thus offer a more robust age estimate for the entire Moenkopi Formation intersected in CPCP-1 cores?

A key component of the CPCP-1 research has involved obtaining numerical age information for parts of the Triassic section along with defining a magnetic polarity zonation to establish a high-resolution chronostratigraphy for the Chinle and Moenkopi formations. Much of the geochronologic work was concentrated

on the Upper Triassic Chinle Formation (Gehrels et al., 2020; and Rasmussen et al., 2020); however, some numerical age estimates have been obtained for parts of the Moenkopi section intersected in core CPCP-1A. A sample from the upper Holbrook Member, about 0.5 m below the Moenkopi/Chinle contact (~405.7 m, msd) was subjected to CA-TIMS U-Pb zircon analysis and yielded a number of young zircons, with a distribution of single crystal ages between ca. 245 and 241 Ma, but no clear coherent age cluster. Gehrels et al. (2020) reported lower precision LA-ICPMS U-Pb zircon data from the same sample and two other samples lower in section within the Holbrook Member and these latter results provided tentative maximum depositional age (MDAs) estimates of 249.5 ± 1.6/2.5 Ma (~448 m, msd) and 248.4 ± 2.0/2.8 Ma (~427.3 m, msd), although these represent mean ages that are not directly comparable with CA-TIMS data. Nonetheless, these data overlap with the LA-ICPMS U-Pb zircon data provided by Riggs et al. (2020), and can still provide conservative age constraints, indicating that the top of the Moenkopi Formation in CPCP-1A is no older than the latest Anisian and the base of the formation is no older than the latest Permian.

The uppermost parts of the Moenkopi polarity record consistently define a normal polarity magnetozone (MF1n, about 0.75 m thick), which is less likely to be a paleo-weathering overprint from the overlying Chinle strata as the NRM intensity and ChRM direction are consistent with the rest of the Moenkopi Formation. We correlate the MF1n magnetozone with MT8 of the latest Anisian/earliest Ladinian stage of the Early and Middle Triassic timescale from Ogg (2012) and Hounslow and Muttoni (2010), and the normal polarity part of chron GD8 of Li et al. (2018); this correlation is consistent with the youngest age peak of the CA-TIMS data from the top of the formation (Figure 12). If we further assume that the magnetic polarity record of the Moenkopi strata obtained in the CPCP-1 cores is essentially complete, and the overall sedimentation rate fluctuated between about 14 m/Myr and 20 m/Myr for most of the Moenkopi sequence, then the oldest reverse polarity zone (MF6r) can be correlated to the reverse polarity magnetozone (LT9) of the latest Olenekian (ca. 247.2 Ma) or Li et al.'s GD2r, in the earliest Anisian. We note that the numerical time scale in Ogg (2012) assumed that the Changhsingian (latest Permian)/Induan boundary had an age of 252.2 Ma, which has now been demonstrated to be at ca. 251.94 to 251.98 Ma (Baresel et al., 2017) or ca. 251.90 Ma (Burgess & Bowring, 2015). The correlation scheme proposed here (Figure 12) is consistent with the fact that the lower half of the Moqui Member and most of the Wupatki Member are dominated by normal polarity magnetozones, as the lower part of the Anisian chrons (MT1 to MT4, Hounslow & Muttoni, 2010; and GD3 to GD4, Li et al., 2018) is dominated by normal polarity. Although such a correlation implies younger ages than those from the LA-ICPMS U-Pb zircon data, it is important to remember that the MDAs do not account for potential uncertainties such as Pb loss and closely spaced but separate zircon age populations. In addition, as samples from detrital sedimentary rocks, these ages could simply be older than the depositional age of each stratum. The relative probability plots of the LA-ICPMS zircon ages are helpful in this regard, as they show the large uncertainties associated with these dates and do overlap with the depositional ages that we infer from the magnetic polarity record. Thus, the dominant peaks as depositional ages can be misleading and may arise entirely from abundant redeposited zircons of that age range, as indicated by the peak at ca. 250 Ma for the 335Y-1 and 349Y-3 samples (Figures 12 and S4).

If, on the other hand, we incorporated the LA-ICPMS zircon MDAs at face value, then most of the Moqui Member and all of the Wupatki Member would be older than about 250.7 Ma and, based on our reported magnetic polarity stratigraphy, the Moenkopi Formation would include the earliest Induan. This correlation model would also require a highly variable sedimentation rate within the Moenkopi Formation and most of the normal polarity-dominated lower Moqui Member would correlate with the reverse polarity dominated Induan and early part of the Olenekian stages. It would also conflict with well-tested lithostratigraphic correlations that indicate the Olenekian marine units of the Moenkopi Formation in southwestern Utah are significantly older than any part of the Moenkopi Formation near PFNP (McKee, 1954; Stewart et al., 1972). In the absence of a high-precision numerical age information for other parts of the Moenkopi Formation, we view this alternative estimate of the age span of the Moenkopi Formation as tenuous and less realistic.

A strong similarity between the magnetic polarity zones obtained in the CPCP-1 cores with the astronomically tuned 405 kyr cycle polarity timescale for the Anisian stage from the Guandao section of South China (Li et al., 2018) suggests that the most parsimonious correlation of the Moenkopi magnetozones MF1n to MF6r would be with the GD8 to GD2r of their study. The magnetochronology correlation suggests that the Moenkopi Formation in the PFNP area of the Colorado Plateau represents the early part of the Middle

Triassic (ca. 247 Ma to 241 Ma) where the depositional age of the Holbrook Member ranges from the middle to latest Anisian (ca. 243.4 Ma to 241 Ma), the Moqui Member from the early to middle Anisian (ca. 246.5 Ma to 243.4 Ma), and the Wupatki Member deposited in the earliest Anisian (ca. 247.0 Ma to 246.5 Ma). Regardless of the possible correlations that might be made between the observed magnetic polarity stratigraphy for the Moenkopi Formation and the geomagnetic polarity timescale, the depositional age estimates for the top of the Moenkopi Formation and the lower Mesa Redondo Member of the Upper Triassic Chinle Formation, based on data from samples from core CPCP-1A (Rasmussen et al., 2020) suggest that the timespan of the regional, pre-Norian disconformity (TR-3) that characterizes this part of North America is about 17 Ma long. The age distribution of the members of the Moenkopi Formation and their thicknesses suggest that the sediment accumulation rate was ∼17 cm/Myr for most of the depositional period with an unusually low (∼5 cm/Myr) during MF2n and MF5r and as high as ∼60 cm/Myr during MF4n (Figure 12). This age model presents a significant revision to the inferred age of the Moenkopi Formation in northeastern Arizona. Whereas the Moenkopi Formation in eastern Arizona was previously thought to be late Olenekian through early Anisian in age (e.g., Lucas & Schoch, 2002; Morales, 1987; Romano et al., 2020; and Steiner et al., 1993), the formation appears to be nearly exclusively Anisian in age, and in particular, extends to the latest Anisian or even earliest Ladinian. Therefore, at least in the Little Colorado River drainage area, the base of the formation is some 1–2 million years younger, and the top of the formation is some 3–4 million years younger, than previously suggested.

6.2. Correlation to Surface Exposures

With our proposed coherent age model for the Moenkopi Formation in the CPCP-1 core, we can make a first attempt at correlating these results to existing magnetostratigraphic data from surface exposures of the formation. Any such effort is necessarily fraught with uncertainty, because published legacy data span 50 years of work, with great variation in approach to data reporting, data quality, and interpretation, as well as significant advances in analytical methods over that time. Specifically, with the Moenkopi Formation in northern Arizona, many of the challenges revolve around short stratigraphic sections with coarse paleomagnetic sampling resolution (e.g., Purucker et al., 1980; and Steiner et al., 1993). Furthermore, some of these studies have misinterpreted the lithostratigraphic placement of sampled sections (see discussion in Nesbitt, 2005a, 2005b, 2005c), leading to unorthodox correlations.

Nonetheless, despite these challenges, using the CPCP-1 age model and marine biostratigraphic constraints as tie points, we suggest a testable hypothesis for correlating these outcrop-based magnetostratigraphic data that is consistent with the accepted lithostratigraphic framework (Figure 13). The polarity record for the Virgin River section in southwestern Utah is critical in this analysis, because of its marine affinity with biostratigraphically informative ammonoids. The lowermost Timpoweap Member (Sinbad Member of some authors) contains a Smithian-aged *Anasibirites* assemblage (Blakey, 1974; Lucas, Goodspeed, et al., 2007; Lucas, Krainer, et al., 2007; and McKee, 1954) and is overlain by strata of the Lower Red Member with a predominantly normal polarity. The uppermost Lower Red Member, overlying Virgin Limestone, and most of the Middle Red Member are of reverse polarity, and crucially, the Virgin Limestone contains late Spathian ammonoids from the *Tirolites-Columbites* assemblage (Hautmann et al., 2013; Poborski, 1954). Therefore, this reverse magnetozone, which is also present at Lees Ferry, most likely correlates to a reverse interval within the CG9-10 and MJ2-3 magnetozones of Li et al. (2018) and Ogg (2012), respectively. This correlation to the polarity timescale is also consistent with lithostratigraphic correlations that indicate the Timpoweap Member, Lower Red Member, Virgin Limestone, and Middle Red Member are all older than the base of the Wupatki Member in the vicinity of PFNP (McKee, 1954; Stewart et al., 1972). A continuous drill core and independent geochronology and magnetostratigraphic study may provide better age constraints of the section and resolve issues with the biostratigraphic age of the Utah section and lateral miscorrelation in the Moenkopi strata.

Purucker et al. (1980) first observed that the base of the lower massive sandstone (LMS) in the Wupatki Member is of normal polarity, and it is directly underlain by a narrow reverse polarity magnetozone. This is fortuitous, because as a laterally persistent blanket deposit, the LMS is a marker bed and recognized over an enormous area from Holbrook, Arizona to St. George, Utah, and has been correlated throughout northern Arizona (Baldwin, 1973; McKee, 1954; Stewart et al., 1972). The LMS unit is clearly present in
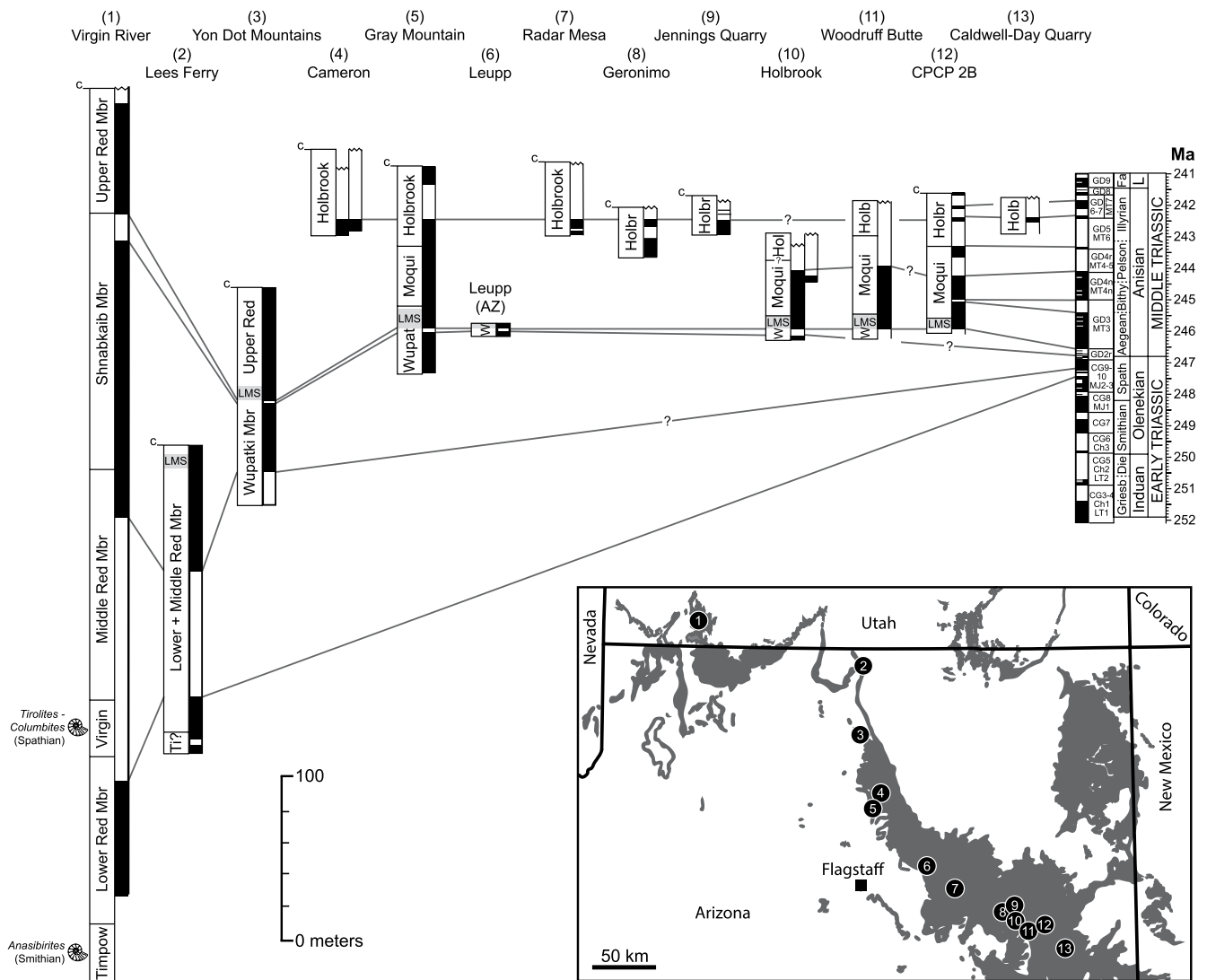
Figure 13. Correlation of the CPCP-2B core magnetostratigraphy to previously published outcrop magnetostratigraphy for the Moenkopi Formation (Steiner et al., 1993) from northern Arizona and southwestern Utah, U.S.A. and the Early-Middle Triassic geomagnetic polarity timescale from Li et al. (2018). Each magnetostratigraphic record is scaled to vertical stratigraphic thickness. Abbreviations: Bithy, Bithynian; Die, Dienerian; Fa, Fassanian; Griesb, Griesbachian; Hol, Holb, Holbr, Holbrook Member; LMS, lower massive sandstone; Pelson—Pelsonian; Spath—Spathian; Timpow, Ti?—Timpoweap Member; and W, Wupat—Wupatki Member.

cores CPCP-1A and CPCP-2B (~216–219 m msd in Figure 12), where it shows a similar magnetic polarity record. Furthermore, this polarity change associated with the LMS is apparent in other sections sampled by Steiner et al. (1993). Thus, this interval provides a useful correlation tie point with a coupled magnetostratigraphic-lithostratigraphic datum, and based on our age model for the CPCP-1 polarity record, correlates to magnetozone GD2r from the earliest Anisian. This magnetozone may also be present in the uppermost Schnabkaib Member at the Virgin River section (Figure 13). North of Leupp, the Wupatki Member contains a considerable thickness of normal polarity strata below this short reverse magnetozone, which likely correlates to a normal polarity zone in the upper Middle Red Member and Schnabkaib Member at Lees Ferry and Virgin River (Figure 13). This hypothesized correlation is consistent with all available data, as it would correlate to the upper normal polarity interval within the CG9-10 and MJ2-3 magnetozones of Li et al. (2018) and Ogg (2012), and would thus fit between the underlying middle-late Spathian reverse magnetozone and overlying earliest Anisian reverse magnetozone.

The overlying Moqui Member is dominated by normal polarity both in outcrop and core and thus is consistent with our correlation of this interval in CPCP-1A and CPCP-2B to GD3n and MT3n of Li et al. (2018) and Ogg (2012). The outcrop-based magnetostratigraphy of the Holbrook Member is the most difficult to correlate, because published records are dominated by very short stratigraphic sections with low-resolution sampling (about 1 sample per meter or lesser resolution) (Steiner et al., 1993). Additionally, the top of the unit is an erosional disconformity and thus differs in age between sites. Nonetheless, these data are broadly consistent with our results from the CPCP-1 core, in that at all sampled sections, the Holbrook Member is dominated by reverse polarity. Thus, outcrop data do not conflict with a late Anisian age for most of this unit, as suggested by our core age model. To the northwest, the Holbrook Member becomes thicker, and the lowermost part is of reverse polarity; these strata could either correlate to one of the short reverse magnetozones in the middle part of the Holbrook Member in the CPCP-1 cores or alternatively to the reverse magnetozone at the top of the Moqui Member. Either option would be consistent with the lithostratigraphy, because it is highly possible that the uppermost gypsum layer that defines the Moqui-Holbrook Member boundary varies in age and stratigraphic position.

Though this hypothesized correlation is not without uncertainty, it agrees with the existing lithostratigraphic framework and helps confirm that key fossil sites in the upper Wupatki Member and Holbrook Member (see Nesbitt, 2005a, 2005c) are all Anisian in age, as implied by our core age model. Correlation of the CPCP-1 age model to other Moenkopi Formation magnetic polarity records from southeastern Utah (Lienert & Helsley, 1980) and western Colorado (Helsley & Steiner, 1974) are more difficult, because these sections are several hundred kilometers north of PFNP with no available data from intervening outcrops, and they do not contain marine index fossils. The very thick (∼230 m) Moenkopi sequence along the Dolores River in western Colorado is predominantly of reverse polarity, with at least five interspersed short normal magnetozones (Helsley & Steiner, 1974). The only parts of the Early-Middle Triassic polarity timescale dominated by reverse polarity are the middle-late Induan through early Smithian, and the late Anisian, but the intervening time is dominated by normal polarity (Hounslow & Muttoni, 2010; Li et al., 2018; Ogg, 2012; Ogg et al., 2020), so how exactly the Dolores section correlates to strata in northern Arizona is unclear. Additionally, this section is located in the Salt Anticline region and sections in these syn-depositional basins caused by salt tectonics may be anomalously expanded relative to other areas. The Hoskinnini Member of the Moenkopi Formation in the vicinity of Bears Ears, southeastern Utah, preserves a reverse polarity magnetozone (Lienert & Helsley, 1980), and this member is inferred based on lithostratigraphic relations to be older than or of the same age as the marine Smithian-aged Timpoweap/Sinbad members (Blakey, 1974). This would suggest a correlation of this unit to either CG6r (Ch3r) or CG7r of the Smithian part of the Early Triassic polarity timescale. The overlying short normal polarity zones at Bears Ears (Lienert & Helsley, 1980) could therefore correlate to any number of normal magnetozones during the late Smithian, Spathian, or early Anisian.

The Anton Chico Member of the Moenkopi Formation in central New Mexico is also difficult to correlate because it is geographically disjunct and comprises relatively thin stratigraphic sections with few polarity reversals/magnetozones (Molina-Garza et al., 1991, 1996; Steiner & Lucas, 1992). The unit has traditionally been correlated with the Holbrook Member in northeastern Arizona because the two members share the temnospondyl amphibian *Eocyclotosaurus* and a number of vertebrate fossil taxa (e.g., Boy et al., 2001; Lucas & Hunt, 1987; Morales, 1987; Rinehart et al., 2015; and Schoch et al., 2010). Available paleomagnetic data are broadly consistent with this correlation, in that the lower Anton Chico Member is normal polarity, whereas the middle-upper part of the unit is reverse polarity, having at least one short normal interval (Molina-Garza et al., 1991, 1996; and Steiner & Lucas, 1992). Thus, the reverse magnetozone likely correlates with some part of MF1r-MF3r in the CPCP cores; the lower Anton Chico normal zone could either correlate with one of the short normal zones in that part of the core or perhaps MF4n at the top of the Moqui Member. If this hypothesized correlation is correct, it would indicate a late Anisian age for the Anton Chico Member.

### 6.3. Implications for Early-Middle Triassic Biostratigraphy and Paleoecology

The proposed revised age of the Moenkopi Formation in northeastern Arizona has considerable implications for the interpretation of its constituent vertebrate fossil assemblages and what they mean in the context of Early-Middle Triassic nonmarine ecosystems worldwide. These new data allow, for the first time,

more robust correlations to other fossil assemblages across Pangea, and therefore test previous biostratigraphic hypotheses. This, in turn, affects how these assemblages document key Triassic biotic events, such as the recovery from the end-Permian mass extinction, the diversification of archosaurian reptiles, and the origin of dinosauromorphs. The Moenkopi exposures of the Little Colorado River drainage preserve two distinct vertebrate body fossil assemblages; one from the upper Wupatki Member and another from the younger Holbrook Member (Lucas & Schoch, 2002; Morales, 1987; Nesbitt, 2005a). The upper Wupatki assemblage was inferred to be late Spathian in age, because it correlates with strata to the northwest that overlay the Spathian Virgin Limestone. The younger Holbrook assemblage was thought to be early Anisian in age, because it contains the temnospondyl amphibian *Eocyclotosaurus*, which is also present in the early Anisian upper Buntsandstein of the Germanic Basin in Europe (Lucas & Schoch, 2002; Morales, 1987; Schoch, 2011), and has been used as an index taxon for nonmarine Anisian age sedimentary rocks (e.g., Lucas, 1998, 2010). Our new age model for the Moenkopi Formation significantly revises the ages of these vertebrate fossils. The upper Wupatki assemblage is now shown to be early Anisian in age (ca. 246 Ma), and the Holbrook assemblage to be late Anisian in age (ca. 243–241 Ma).

Among western North American fossil assemblages, the Chugwater Group of Wyoming is often geologically and paleontologically compared to the Moenkopi Formation, as this sequence preserves similar red bed facies that have been the focus of paleomagnetic studies (e.g., Shive et al., 1984). Typically, the Wupatki Member in Arizona has been considered age-equivalent with the upper Red Peak Formation in Wyoming and both share similar vertebrate footprint assemblages (e.g., Lovelace & Lovelace, 2012; Thomson & Lovelace, 2014). We can now demonstrate that the lower Anisian Wupatki Member, and its vertebrate trace and body fossil assemblages (e.g., Peabody, 1948), is definitively younger than any part of the Red Peak Formation, because the top of the latter unit can be no younger than latest Spathian (Hounslow & Muttoni, 2010; Lovelace & Doebbert, 2015). Thus, the Wupatki Member is more likely to correlate with the younger Crow Mountain Formation of the Chugwater Group. This might even suggest that the poorly dated "unnamed red beds" of the upper Chugwater Group, which produce important reptile body fossils such as rhynchosaurian archosauromorphs and the "rauisuchian" pseudosuchian archosaur *Heptasuchus clarki* (Nesbitt et al., 2020), might be of a similar age to the Holbrook Member of the Moenkopi Formation.

At a broader geographic scale, the revised ages for the Moenkopi Formation of northeastern Arizona require a reevaluation of the intercontinental vertebrate biostratigraphic correlations that were originally used to date the Moenkopi Formation in northeastern Arizona. In particular, the Moenkopi has traditionally been correlated with two European units, the Helsby Sandstone Formation (previously known as the Otter/Bromsgrove Sandstone–see Ambrose et al., 2014) in England and the Buntsandstein in the Germanic Basin (Lucas 1998, 2010; Lucas & Schoch, 2002; Morales, 1987; Rayfield et al., 2005; Romano et al., 2020). Fortuitously, both of these European sequences have magnetostratigraphic age constraints (e.g., Hounslow & McIntosh, 2003; Hounslow & Muttoni, 2010; Szurlies, 2004, 2007), allowing for a direct comparison with our Moenkopi age model (Figure 14). In addition, these units possess similar nonmarine tetrapod assemblages, including diverse and abundant capitosaurian temnospondyl amphibians, procolophonid parareptiles, tanystropheid archosauromorph reptiles, and peculiar sail-backed pseudosuchian archosaurs called ctenosauriscids (e.g., Benton, 2011; Benton et al., 1994; Butler et al., 2011; Coram et al., 2019; Fraser & Rieppel, 2006; Milner et al., 1990; Nesbitt, 2003, 2005a; 2005c; Säilä, 2008; Schoch, 2011; Spencer & Isaac, 1983; Spencer & Storrs, 2002; and Sues & Reisz, 2008). Previously, the inferred Spathian (late Olenekian) age of the Wupatki assemblage meant that it was correlated with the vertebrate assemblage of the Hardegsen and lower Solling formations of the Buntsandstein (e.g., Lucas & Schoch, 2002). Although these two areas do not share any taxa at the genus or species level, they both contain similar trematosaurian and paracyclotosaurian temnospondyl amphibians. With our revised age constraints, the Wupatki Member now correlates with younger levels in the Buntsandstein, specifically the lower Röt Formation (Figure 14).

The revised age for the Holbrook Member not only affects correlation with western European vertebrate fossil records, but also the use of some of the taxa in these assemblages for global biostratigraphy. The shared presence of the capitosaurian temnospondyl *Eocyclotosaurus* meant that the Holbrook assemblage was correlated to the middle-upper Röt Formation and equivalents in the Buntsandstein (Lucas, 1998, 2010; Lucas & Schoch, 2002). Now, we can demonstrate that the Holbrook Member fossils are much younger (late Anisian), and in fact correlate with the marine lower Muschelkalk in Germany. This revised age
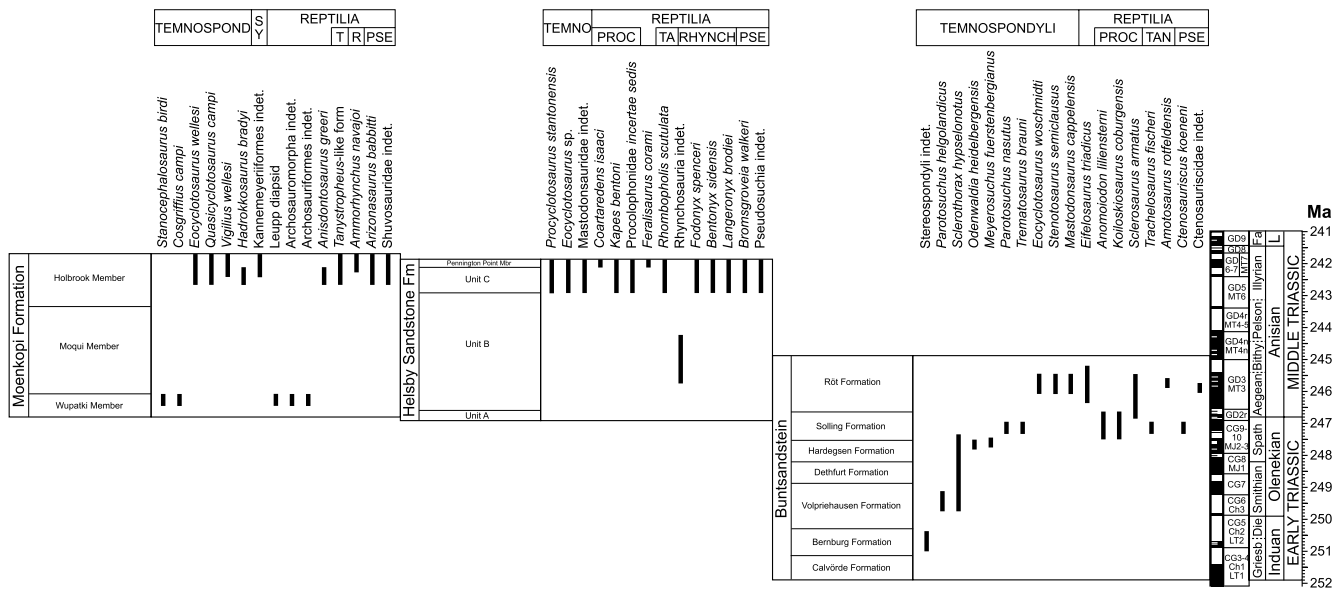
Figure 14. Nonmarine tetrapod biostratigraphy of key Northern Hemisphere units based on magnetostratigraphic age constraints and their correlation to the Early-Middle Triassic geomagnetic polarity timescale from Li et al. (2018). Correlations based on Szurlies (2004, 2007), Hounslow and McIntosh (2003), Hounslow and Muttoni (2010), and this work. Abbreviations: Bithy—Bithynian; Die—Dienerian; Fa—Fassanian; Griesb—Griesbachian; Pelson—Pelsonian; Proc—Procolophonidae; Pse—Pseudosuchia; R, Rhynch—Rhynchosauria; Spath—Spathian; Sy—Synapsida; T, Ta, Tan—Tanystropheidae; and Temno, Temnospond—Temnospondyli.

also indicates that the Holbrook assemblage correlates with the vertebrate fossil-bearing part of the Helsby Sandstone Formation, which also preserves specimens of *Eocyclotosaurus*, and is late Anisian in age (Figure 14). These two units also share the presence of closely related species of rhynchosaurian archosauromorphs, ctenosauriscid pseudosuchian archosaurs, but differ in the absence (to date) of procolophonids in the Holbrook Member. More broadly, these results demonstrate that although *Eocyclotosaurus* might be a nonmarine index taxon of the Anisian Stage, it is not diagnostic of the early Anisian (*contra* Lucas & Schoch, 2002). This reinforces a number of recent studies that demonstrate difficulties in using Triassic nonmarine vertebrates for biostratigraphy in the absence of precise nonbiostratigraphic age constraints (e.g., Irmis et al., 2010, 2011; Langer et al., 2018; Marsicano et al., 2016; Ottone et al., 2014; Rasmussen et al., 2020; Rayfield et al., 2005, 2009; Schultz, 2005). Elsewhere in the Tethys region, capitosaurian temnospondyl amphibian fossils from the Catalonian Basin of the northeastern Iberian Peninsula (Fortuny, Bolet, et al., 2011; Fortuny, Galobart, et al., 2011) are dated to the early Anisian based on palynomorph biostratigraphy and magnetostratigraphy (Dinarès-Turell et al., 2005). This suggests they are approximately equivalent in age to the Wupatki vertebrate assemblage, though the known taxa from each area (i.e., *Calmasuchus* from Spain and *Stanocephalosaurus* from Arizona) are not closely related (cf. Fortuny, Galobart, et al., 2011: Figure 7).

Comparisons with most other Middle Triassic nonmarine vertebrate assemblages are difficult because of the lack of precise nonbiostratigraphic age constraints (Marsicano et al., 2016; Ottone et al., 2014). One exception is the Ordos Basin from the North China Block, where Middle Triassic vertebrate fossils are constrained by high-resolution CA-TIMS U-Pb zircon ages (Liu et al., 2018) (some paleomagnetic studies have been conducted, but not in a stratigraphic context; cf. Yang et al., 1991). These dates indicate that the Emaying Formation and lower Tongchuan Formation are late Anisian in age, penecontemporaneous with the Holbrook Member of the Moenkopi Formation. This Ordos Basin assemblage (the "*Sinokannemeyeria* fauna") differs from that of the Holbrook Member in the abundance and diversity of synapsids (kannemeyeriiform dicynodonts, therocephalians, and non-mammaliaform cynodonts), rarity of temnospondyls, and abundance of early archosauriforms (i.e., *Shansisuchus*) (Liu, 2015; Liu & Abdala, 2015; Liu & Sullivan, 2017; and Liu et al., 2015, 2018). Nonetheless, the Ermaying Formation does preserve some remains of pseudosuchian archosaurs, including a shuvosaurid (Liu et al., 2015; Liu & Sullivan, 2017), a lineage also present in the Holbrook Member (Figure 14; Nesbitt, 2005b). Intriguingly, the underlying Heshanggou Formation, which

is typically assigned an Olenekian age, preserves the ctenosauriscid archosaur *Xilousuchus*, procolophonid parareptiles, therocephalians, kannemeyeriiform dicynodonts, and temnospondyls (e.g., Liu et al., 2018; Nesbitt et al., 2011). Given the late Anisian age for the Ermaying Formation, it is possible that the Heshanggou assemblage is in fact early Anisian in age, though this remains to be confirmed (Liu et al., 2018). The presence of ctenosauriscids and procolophonids in this older assemblage is a feature shared in common with the magnetostratigraphically dated Anisian Moenkopi, Helsby Sandstone, and Buntsandstein vertebrate records (Figure 14).

Classic "Anisian" Gondwanan vertebrate assemblages such as those correlated to the *Cynognathus* Assemblage Zone (e.g., Bandyopadhyay & Sengupta, 1999; Hancox et al., 2020; Kutty et al., 1987; Peecook et al., 2017; Sidor et al., 2013, 2014) remain unconstrained by biostratigraphically independent ages, and thus it is unclear if they are actually assignable to the Anisian Stage (see discussion in Peecook et al., 2017). This uncertainty is particularly acute given that a number of "Middle Triassic" assemblages have been recently radioisotopically dated to much younger ages (e.g., Langer et al., 2018; Marsicano et al., 2016; Ottone et al., 2014). Thus, it is difficult to compare these fossil records with those of the Moenkopi Formation when their age is so uncertain.

From a broader macroevolutionary perspective, the revised age model of the Moenkopi Formation (and its context among other fossil assemblages) has important implications for understanding Early-Middle Triassic biotic events. On one hand, the revised age model suggests the fossil assemblages are too late in time to document the recovery from the end-Permian mass extinction documented in marine and terrestrial ecosystems (cf. Irmis & Whiteside, 2012; Payne et al., 2004). In contrast, taken together with other well-dated Anisian assemblages (e.g., Helsby Sandstone and Buntsandstein), the age model demonstrates that the Triassic archosauromorph reptile radiation was well under way by the beginning of the Anisian, with multiple documented lineages of rhynchosaurs, tanystropheids, early archosauriforms, and pseudosuchian archosaurs. In particular, the presence of ctenosauriscid pseudosuchian archosaurs in several units shows that both crocodile-line (Pseudosuchia) and bird-line (Avemetatarsalia) archosaurs, two lineages that dominated terrestrial ecosystems for the rest of the Mesozoic Era, had diverged and begun to diversify prior to the Anisian. The Anisian is also typically identified as the time when dinosauromorphs first originated (e.g., Langer et al., 2013; Li et al., 2018; Nesbitt et al., 2010, 2012, 2017), but this is based on fossils from East Africa whose age is uncertain (see previous paragraph). In addition, the trackmaker of putative dinosauromorph footprints from the Early-Middle Triassic is actually ambiguous (Langer et al., 2013; Padian, 2013). Thus, the conspicuous absence of unambiguous dinosauromorph fossils from well-dated Anisian vertebrate assemblages in the Northern Hemisphere is significant; it suggests that either dinosauromorph origins postdate the Anisian, or that Anisian dinosauromorphs were rare if not absent in the low to mid-latitudes of the Northern Hemisphere.

7. Conclusions

The continuous coring project CPCP-1 Scientific Drilling at Petrified Forest National Park provided the opportunity to establish a complete magnetic polarity record for the ~88- m-thick sequence of Moenkopi Formation strata intersected in the two cores (CPCP-1A and CPCP-2B), which would be otherwise unattainable from surface exposure due to inaccessibility, punctuated exposures, and/or chemical alteration. This study shows good agreement between the polarity records obtained from the Moenkopi strata from the two cores (about 30 km apart) and an overall similarity with comparable marine and terrestrial sections, and with the previous studies across the depositional basin of the Moenkopi Formation. Examination of the magnetozones from the CPCP-1 strata in the context of the combined Early to Middle Triassic geomagnetic polarity time scale from Ogg (2012), Hounslow and Muttoni (2010), and Li et al. (2018) in concert with the CA-TIMS U-Pb age of 241.38 ± 0.43 Ma from the uppermost part of the Holbrook Member suggests that the Moenkopi strata were deposited almost entirely during the Anisian (ca. 247.0 Ma to 241.5 Ma), which provides an independent, non-biostratigraphic age constraint for this important, regionally extensive Mesozoic epicontinental basin sequence. The magnetochronology records from the Moenkopi Formation and from the disconformably overlying Chinle Formation give credence to an estimated time duration of about 17 Ma for the regional hiatus within the Triassic sequence present in the Colorado Plateau area. The new age model also demonstrates that Moenkopi Formation vertebrate fossil assemblages are several millions of

years (some 3 to 4 Ma) younger than previously suggested, changing their implications for understanding nonmarine recovery from the end-Permian mass extinction and use for intercontinental vertebrate biostratigraphy. Thus, the proposed magnetic polarity correlation model from this study, although tied to limited numerical age data, for the Moenkopi sections intersected in CPCP-1, offers a testable contribution for high-resolution age correlation for terrestrial Middle Triassic strata in future paleoclimatic studies, precise stratigraphic position of major global biotic transitions, and refinement of lithostratigraphic and biostratigraphic correlations of Middle Triassic strata on a global basis. This new age determination will also require a revision of the North American paleomagnetic pole compilations involving Moenkopi Formation data.

Data Availability Statement

Data sets for this research have been uploaded into DRYAD data repository. This data set has been assigned a unique identifier and can be downloaded using the following links: https://doi.org/10.5061/dryad.fbg79c-nv1 for the thermal demagnetization data and https://doi.org/10.5061/dryad.v41ns1rwj for the anisotropy of magnetic susceptibility (AMS) data.

References

Ambrose, K., Hough, E., Smith, N. J. P., & Warrington, G. (2014). Lithostratigraphy of the Sherwood Sandstone Group of England, Wales and south-west Scotland. *British Geological Survey Geology and Regional Geophysics Directorate Research Report*, *14*, 1-50.

Arason, Þ., & Levi, S. (2010). Maximum likelihood solution for inclination-only data in paleomagnetism. *Geophysical Journal International*, *182*(2), 753–771. https://doi.org/10.1111/j.1365-246x.2010.04671.x

Ash, S. R., & Morales, M. (1993). Anisian plants from Arizona: The oldest Mesozoic megaflora in North America. *New Mexico Museum of Natural History & Science Bulletin*, *3*, 27–29.

Baldwin, E. J. (1973). The Moenkopi Formation of north-central Arizona; an interpretation of ancient environments based upon sedimentary structures and stratification types. *Journal of Sedimentary Research*, *43*(1), 92–106. https://doi.org/10.1306/74d726ee-2b21-11d7-8648000102c1865d

Bandyopadhyay, S., & Sengupta, D. P. (1999). Middle Triassic vertebrates of India. *Journal of African Earth Sciences*, *29*(1), 233–241. https://doi.org/10.1016/s0899-5362(99)00093-7

Baresel, B., Bucher, H., Brosse, M., Cordey, F., Guodun, K., & Schaltegger, U. (2017). Precise age for the Permian–Triassic boundary in South China from high-precision U-Pb geochronology and Bayesian age–depth modeling. *Solid Earth*, *8*(2), 361–378.

Benton, M. J. (2011). Archosaur remains from the Otter Sandstone Formation (Middle Triassic, late Anisian) of Devon, southern UK. *Proceedings of the Geologists' Association*, *122*(1), 25–33. https://doi.org/10.1016/j.pgeola.2010.08.004

Benton, M. J., Warrington, G., Newell, A. J., and Spencer, P. S. (1994). A review of the British Middle Triassic tetrapod assemblages In *The shadow of the dinosaurs: Early Mesozoic tetrapods*, edited by In N. C. Fraser and H.-D. Sues (Eds.), pp. 131–160, Cambridge University Press.

Blackburn, T. J., Olsen, P. E., Bowring, S. A., McLean, N. M., Kent, D. V., Puffer, J., et al. (2013). Zircon U-Pb geochronology links the end-Triassic extinction with the Central Atlantic Magmatic Province. *Science*, *340*(6135), 941–945. https://doi.org/10.1126/science.1234204

Blakey, R. C. (1973). Stratigraphy and origin of the Moenkopi Formation (Triassic) of southeastern Utah. *Mountain Geologist*, *10*, 1–17.

Blakey, R. C. (1974). Stratigraphic and depositional analysis of the Moenkopi Formation, southeastern Utah. *Utah Geological Survey Bulletin*, *104*, 1–81. https://doi.org/10.34191/b-104

Blakey, R. C. (2008). Gondwana paleogeography from assembly to breakup—A 500 my odyssey. *Geological Society of America Special Paper*, *441*, 1–28. https://doi.org/10.1130/2008.2441(01)

Blakey, R. C., & Gubitosa, R. (1983). Late Triassic paleogeography and depositional history of the Chinle Formation, southern Utah and northern Arizona. In M. W. Reynolds & E. D. Dolly (Eds.), *Mesozoic paleogeography of the west-Central United States*, Society of Economic Paleontologists and Mineralogists, Rocky mountain section (Vol. 2, pp. 57–76).

Boy, J. A., Schoch, R. R., & Lucas, S. G. (2001). The Moenkopi Formation in east-central New Mexico: Stratigraphy and vertebrate fauna. *New Mexico Geological Society Guidebook*, *52*, 103–109.

Brotherton, J. L., Chowdhury, N. U. M. K., & Sweet, D. E. (2020). A synthesis of late Paleozoic sedimentation in central and eastern New Mexico: Implications for timing of Ancestral Rocky Mountains deformation. *Late Paleozoic and early Mesozoic tectonostratigraphy and biostratigraphy of western Pangea*.SEPM Special Publication, 113,

Buhedma, H. (2017). *Magnetostratigraphy of the Chinle and Moenkopi strata cored at Colorado Plateau Coring project site 1A, Northern Petrified Forest National Park* (MS thesis). Retrieved from Eugene McDermott Library. Richardson, TX: The University of Texas at Dallas.

Burgess, S. D., & Bowring, S. A. (2015). High-precision geochronology confirms voluminous magmatism before, during, and after Earth's most severe extinction. *Science advances*, *1*(7), e1500470. https://doi.org/10.1126/sciadv.1500470

Butler, R. F. (1982). Magnetic mineralogy of continental deposits, San Juan Basin, New Mexico, and Clark's Fork Basin, Wyoming. *Journal of Geophysical Research*, *87*(B9), 7843–7852. https://doi.org/10.1029/jb087ib09p07843

Butler, R. J., Brusatte, S. L., Reich, M., Nesbitt, S. J., Schoch, R. R., & Hornung, J. J. (2011). The sail-backed reptile *Ctenosauriscus* from the latest Early Triassic of Germany and the timing and biogeography of the early archosaur radiation. *PLoS One*, *6*(10), 1–28, e25693. https://doi.org/10.1371/journal.pone.0025693

Colbert, E. H., & Gregory, J. T. (1957). Correlation of continental Triassic sediments by vertebrate fossils. *The Geological Society of America Bulletin*, *68*, 1456–1467.

Collinson, D. W. (1975). Instruments and techniques in paleomagnetism and rock magnetism. *Reviews of Geophysics*, *13*(5), 659–686. https://doi.org/10.1029/rg013i005p00659

Coram, R. A., Radley, J. D., & Benton, M. J. (2019). The Middle Triassic (Anisian) Otter Sandstone biota (Devon, UK): Review, recent discoveries and ways ahead. *Proceedings of the Geologists' Association*, *130*, 294–306. https://doi.org/10.1016/j.pgeola.2017.06.007

Dickinson, W. R., & Gehrels, G. E. (2009). Use of U–Pb ages of detrital zircons to infer maximum depositional ages of strata: A test against a Colorado Plateau Mesozoic database. *Earth and Planetary Science Letters*, *288*(1–2), 115–125. https://doi.org/10.1016/j.epsl.2009.09.013

Dinarès-Turell, J., Diez, J. B., Rey, D., & Arnal, I. (2005). Buntsandstein″ magnetostratigraphy and biostratigraphic reappraisal from eastern Iberia: Early and Middle Triassic stage boundary definitions through correlation to Tethyan sections. *Palaeogeography, Palaeoclimatology, Palaeoecology*, *229*, 158–177. https://doi.org/10.1016/j.palaeo.2005.06.036

Elston, D. P., & Purucker, M. E. (1979). Detrital magnetization in red beds of the Moenkopi Formation (Triassic), Gray Mountain, Arizona. *Journal of Geophysical Research B*, *84*(B4), 1653–1665. https://doi.org/10.1029/jb084ib04p01653

Fortuny, J., Bolet, A., Sellés, A. G., Cartanyà, J., & Galobart, À. (2011). New insights on the Permian and Triassic vertebrates from the Iberian Peninsula with emphasis on the Pyrenean and Catalonian basins. *Journal of Iberian Geology*, *37*(1), 65–86.

Fortuny, J., Galobart, À., & De Santisteban, C. (2011). A new capitosaur from the Middle Triassic of Spain and the relationships within the Capitosauria. *Acta Palaeontologica Polonica*, *56*(3), 553–566. https://doi.org/10.4202/app.2010.0025

Fraser, N. C., & Rieppel, O. (2006). A new protorosaur (Diapsida) from the upper Buntsandstein of the Black Forest, Germany. *Journal of Vertebrate Paleontology*, *26*(4), 866–871. https://doi.org/10.1671/0272-4634(2006)26[866:anpdft]2.0.co;2

Gehrels, G., Giesler, D., Olsen, P., Kent, D., Marsh, A., Parker, W., & Lepre, C. (2020). LA-ICPMS U-Pb geochronology of detrital zircon grains from the Coconino, Moenkopi, and Chinle formations in the Petrified Forest National Park (Arizona). *Geochronology*, *2*, 257–282. https://doi.org/10.5194/gchron-2-257-2020

Hancox, P. J., Neveling, J., & Rubidge, B. S. (2020). Biostratigraphy of the Cynognathus assemblage zone (Beaufort Group, Karoo Supergroup), South Africa. *South African Journal of Geology*, *123*(2), 217–238. https://doi.org/10.25131/sajg.123.0016

Haque, Z., Geissman, J. W., Buhedma, H., & Olsen, P. E. (2019). Magnetic polarity stratigraphy and rock magnetism of the continuous cores of the Triassic Moenkopi Formation strata recovered from the Colorado Plateau Coring Project (CPCP) Phase I. *Geological Society of America Abstracts with Programs*, *51*(5).

Haque, Z, Geissman, J. W., DeCelles, P. G., & Carrapa, B. (2021). A magnetostratigraphic age constraint for the proximal synorogenic conglomerates of the Late Cretaceous Cordilleran foreland basin, northeast Utah, USA. *Geological Society of America Bulletin*, *133*, (9-10), 1795–1814. http://dx.doi.org/10.1130/b35768.1

Haque, Z., Geissman, J. W., & Olsen, P. E. (2018). Magnetic polarity stratigraphy and rock magnetic data from Moenkopi Formation strata cored at site PFNP-13-2B, a continuous record of Triassic strata, Colorado Plateau Coring Project. Presented at American Geophysical Union, Fall Meeting (abstract #GP43B-0776).

Hautmann, M., Smith, A. B., McGowan, A. J., & Bucher, H. (2013). Bivalves from the Olenekian (Early Triassic) of south-western Utah: Systematics and evolutionary significance. *Journal of Systematic Palaeontology*, *11*(3), 263–293. https://doi.org/10.1080/14772019.2011.637516

Heckert, A. B., & Lucas, S. G. (2002). Revised Upper Triassic stratigraphy of the Petrified Forest National Park, Arizona, USA. *New Mexico Museum of Natural History and Science Bulletin*, *21*, 1–36.

Helsley, C. E., & Steiner, M. B. (1974). Paleomagnetism of the lower Triassic Moenkopi formation. *The Geological Society of America Bulletin*, *85*(3), 457–464. https://doi.org/10.1130/0016-7606(1974)85<457:potltm>2.0.co;2

Herriott, T. M., Crowley, J. L., Schmitz, M. D., Wartes, M. A., & Gillis, R. J. (2019). Exploring the law of detrital zircon: LA-ICP-MS and CA-TIMS geochronology of Jurassic forearc strata, Cook Inlet, Alaska, USA. *Geology*, *47*(11), 1044–1048. https://doi.org/10.1130/g46312.1

Hounslow, M. W., & McIntosh, G. (2003). Magnetostratigraphy of the Sherwood Sandstone Group (Lower and Middle Triassic), south Devon, UK: Detailed correlation of the marine and non-marine Anisian. *Palaeogeography, Palaeoclimatology, Palaeoecology*, *193*(2), 325–348. https://doi.org/10.1016/s0031-0182(03)00235-9

Hounslow, M. W., & Muttoni, G. (2010). The geomagnetic polarity timescale for the Triassic: Linkage to stage boundary definitions. *Geological Society, London, Special Publications*, *334*(1), 61–102. https://doi.org/10.1144/sp334.4

Hrouda, F. (1982). Magnetic Anisotropy and its Application in Geology and Geophysics. *Geophysical Surveys*, *5*, 37–82. https://doi.org/10.1007/bf01450244

Irmis, R. B., Martz, J. W., Parker, W. G., & Nesbitt, S. J. (2010). Re-evaluating the correlation between Late Triassic terrestrial vertebrate biostratigraphy and the GSSP-defined marine stages. *Albertiana*, *38*, 40–52.

Irmis, R. B., Mundil, R., Martz, J. W., & Parker, W. G. (2011). High-resolution U–Pb ages from the Upper Triassic Chinle Formation (New Mexico, USA) support a diachronous rise of dinosaurs. *Earth and Planetary Science Letters*, *309*(3–4), 258–267. https://doi.org/10.1016/j.epsl.2011.07.015

Irmis, R. B., & Whiteside, J. H. (2012). Delayed recovery of non-marine tetrapods after the end-Permian mass extinction tracks global carbon cycle. *Proceedings of the Royal Society of London, Biological Sciences*, *279*, 1310–1318. https://doi.org/10.1098/rspb.2011.1895

Kent, D. V., & Irving, E. (2010). Influence of inclination error in sedimentary rocks on the Triassic and Jurassic apparent pole wander path for North America and implications for Cordilleran tectonics. *Journal of Geophysical Research*, *115*(B10). https://doi.org/10.1029/2009jb007205

Kent, D. V., Olsen, P. E., Lepre, C., Rasmussen, C., Mundil, R., Gehrels, G. E., et al. (2019). Magnetochronology of the entire Chinle Formation (Norian age) in a scientific drill core from Petrified Forest National Park (Arizona, USA) and implications for regional and global correlations in the Late Triassic. *Geochemistry, Geophysics, Geosystems*, *20*(11), 4654–4664. https://doi.org/10.1029/2019gc008474

Kent, D. V., Olsen, P. E., & Muttoni, G. (2017). Astrochronostratigraphic polarity time scale (APTS) for the Late Triassic and Early Jurassic from continental sediments and correlation with standard marine stages. *Earth-Science Reviews*, *166*, 153–180. https://doi.org/10.1016/j.earscirev.2016.12.014

Kent, D. V., Olsen, P. E., Rasmussen, C., Lepre, C., Mundil, R., Irmis, R. B., et al. (2018). Empirical evidence for stability of the 405-kiloyear Jupiter–Venus eccentricity cycle over hundreds of millions of years. *Proceedings of the National Academy of Sciences*, *115*(24), 6153–6158. https://doi.org/10.1073/pnas.1800891115

Kirschvink, J. L. (1980). The least-squares line and plane and the analysis of paleomagnetic data. *Geophysical Journal International*, *62*(3), 699–718. https://doi.org/10.1111/j.1365-246x.1980.tb02601.x

Kluth, C. F., & Coney, P. J. (1983). Comment and reply on 'plate tectonics of the Ancestral Rocky Mountains' REPLY. *Geology*, *11*(2), 121–122. https://doi.org/10.1130/0091-7613(1983)11<121:caropt>2.0.co;2

Kodama, K. P. (2012). *Paleomagnetism of sedimentary rocks: Process and interpretation*. John Wiley & Sons.

Kutty, T. S., Jain, S. L., & Roy Chowdhury, T. (1987). Gondwana sequence of the northern Pranhita-Godavari Valley: Its stratigraphy and vertebrate faunas. *Palaeobotanist*, *36*, 214–229

Langer, M. C., Nesbitt, S. J., Bittencourt, J. S., & Irmis, R. B. (2013). Non-dinosaurian Dinosauromorpha. *Geological Society, London, Special Publications*, *379*, 157–186. https://doi.org/10.1144/sp379.9

Langer, M. C., Ramezani, J., & Da Rosa, Á. A. S. (2018). U-Pb age constraints on dinosaur rise from south Brazil. *Gondwana Research*, *57*, 133–140. https://doi.org/10.1016/j.gr.2018.01.005

Lehrmann, D. J., Stepchinski, L., Altiner, D., Orchard, M. J., Montgomery, P., Enos, P., et al. (2015). An integrated biostratigraphy (conodonts and foraminifers) and chronostratigraphy (paleomagnetic reversals, magnetic susceptibility, elemental chemistry, carbon isotopes and geochronology) for the Permian–Upper Triassic strata of Guandao section, Nanpanjiang Basin, south China. *Journal of Asian Earth Sciences*, *108*, 117–135. https://doi.org/10.1016/j.jseaes.2015.04.030

Li, M., Huang, C., Hinnov, L., Chen, W., James, O., & Tian, W. (2018). Astrochronology of the Anisian stage (Middle Triassic) at the Guandao reference section, South China. *Earth Planetary Science Letters*, *482*, 591–606. https://doi.org/10.1016/j.epsl.2017.11.042

Liebes, E., & Shive, P. N. (1982). Magnetization acquisition in two Mesozoic red sandstones. *Physics of the Earth and Planetary Interiors*, *30*(4), 396–404. https://doi.org/10.1016/0031-9201(82)90049-8

Lienert, B. R., & Helsley, C. E. (1980). Magnetostratigraphy of the Moenkopi Formation at Bears Ears, Utah. *Journal of Geophysical Research*, *85*(B3), 1475–1480. https://doi.org/10.1029/jb085ib03p01475

Liu, J. (2015). New discoveries from the *Sinokannemeyeria-Shansisuchus* assemblage zone: 1. Kannemeyeriiformes from Shanxi, China. *Vertebrata Palasiatica*, *53*(1), 16–28.

Liu, J., & Abdala, F. (2015). New discoveries from the *Sinokannemeyeria-Shansisuchus* assemblage zone: 2. A new species of *Nothogomphodon* (Therapsida - Therocephalia) from the Ermaying Formation of Shanxi, China. *Vertebrata Palasiatica*, *53*(2), 123–132.

Liu, J., Butler, R., Sullivan, C., & Ezcurra, M. D. (2015). 'Chasmatosaurus ultimus,' a putative proterosuchid archosauriform from the Middle Triassic, is an indeterminate crown archosaur. *Journal of Vertebrate Paleontology*, 1–5, e965779. https://doi.org/10.1080/02724634.2015.965779

Liu, J., Ramezani, J., Li, L., Shang, Q.-H., Xu, G.-H., Wang, Y.-Y., & Yang, J.-S. (2018). High-precision temporal calibration of Middle Triassic vertebrate biostratigraphy: U-Pb zircon constraints for the *Sinokannemeyeria* fauna and *Yonghesuchus*. *Vertebrata Palasiatica*, *56*(1), 16–24.

Liu, J., & Sullivan, C. (2017). New discoveries from the *Sinokannemeyeria-Shansisuchus* assemblage zone: 3. Archosauriformes from Linxian, Shanxi, China. *Vertebrata Palasiatica*, *55*(2), 110–128.

Lovelace, D. M., & Doebbert, A. C. (2015). A new age constraint for the Early Triassic Alcova Limestone (Chugwater), Wyoming. *Palaeogeography, Palaeoclimatology, Palaeoecology*, *424*, 1–5. https://doi.org/10.1016/j.palaeo.2015.02.009

Lovelace, D. M., & Lovelace, S. D. (2012). Paleoenvironments and paleoecology of a Lower Triassic invertebrate and vertebrate ichnoassemblage from the Red Peak Formation (Chugwater Group), central Wyoming. *PALAIOS*, *27*, 636–657. https://doi.org/10.2110/palo.2012.p12-011r

Lowrie, W. (1990). Identification of ferromagnetic minerals in a rock by coercivity and unblocking temperature properties. *Geophysical Research Letters*, *17*(2), 159–162. https://doi.org/10.1029/gl017i002p00159

Lucas, S. G. (1998). Global Triassic tetrapod biostratigraphy and biochronology. *Palaeogeography, Palaeoclimatology, Palaeoecology*, *143*, 347–384. https://doi.org/10.1016/s0031-0182(98)00117-5

Lucas, S. G. (2010). The Triassic timescale based on nonmarine tetrapod biostratigraphy and biochronology. *Geological Society, London, Special Publications*, *334*, 447–500. https://doi.org/10.1144/sp334.15

Lucas, S. G., Goodspeed, T. H., & Estep, J. W. (2007). Ammonoid biostratigraphy of the Lower Triassic Sinbad Formation, east-central Utah. *New Mexico Museum of Natural History & Science Bulletin*, *40*, 103–108.

Lucas, S. G., & Hunt, A. P. (1987). Stratigraphy of the Anton Chico and Santa Rosa formations, Triassic of east-central New Mexico. *Journal of the Arizona-Nevada Academy of Science*, *22*, 21–33.

Lucas, S. G., Krainer, K., & Milner, A. R. C. (2007). The type section and age of the Timpoweap Member and stratigraphic nomenclature of the Triassic Moenkopi Group in southwestern Utah. *New Mexico Museum of Natural History & Science Bulletin*, *40*, 109–117.

Lucas, S. G., & Schoch, R. R. (2002). Triassic temnospondyl biostratigraphy, biochronology and correlation of the German Buntsandstein and North American Moenkopi Formation. *Lethaia*, *35*(2), 97–106. https://doi.org/10.1080/002411602320183962

Marsicano, C. A., Irmis, R. B., Mancuso, A. C., Mundil, R., & Chemale, F. (2016). The precise temporal calibration of dinosaur origins. *Proceedings of the National Academy of Sciences*, *113*(3), 509–513. https://doi.org/10.1073/pnas.1512541112

Martz, J. W., & Parker, W. G. (2010). Revised lithostratigraphy of the Sonsela Member (Chinle Formation, Upper Triassic) in the southern part of Petrified Forest National Park, Arizona. *PLoS One*, *5*(2), e9329. https://doi.org/10.1371/journal.pone.0009329

Martz, J. W., Parker, W. G., Skinner, L., Raucci, J. J., Umhoefer, P., & Blakey, R. C. (2013). Geologic map of Petrified Forest National Park, Arizona. *Arizona Geological Survey Contributed Map*, *CM-12-A*, 1–18.

McFadden, P. L., & Reid, A. B. (1982). Analysis of palaeomagnetic inclination data. *Geophysical Journal International*, *69*(2), 307–319. https://doi.org/10.1111/j.1365-246x.1982.tb04950.x

McKee, E. D. (1954). Stratigraphy and history of the Moenkopi Formation of Triassic age. *Geological Society of America Memoir*, *61*, 1–126. https://doi.org/10.1130/mem61-p1

Milner, A. R., Gardiner, B. G., Fraser, N. C., & Taylor, M. A. (1990). Vertebrates from the Middle Triassic Otter Sandstone Formation of Devon. *Palaeontology*, *33*(4), 873–892.

Molina-Garza, R. S., Geissman, J. W., Lucas, S. G., & Van der Voo, R. (1996). Palaeomagnetism and magnetostratigraphy of Triassic strata in the Sangre de Cristo Mountains and Tucumcari Basin, New Mexico, USA. *Geophysical Journal International*, *124*, 935–953. https://doi.org/10.1111/j.1365-246x.1996.tb05646.x

Molina-Garza, R. S., Geissman, J. W., Van der Voo, R., Lucas, S. G., & Hayden, S. N. (1991). Paleomagnetism of the Moenkopi and Chinle Formations in central New Mexico: Implications for the North American apparent polar wander path and Triassic magnetostratigraphy. *Journal of Geophysical Research*, *96*(B9), 14239–14262.

Morales, M. (1987). Terrestrial fauna and flora from the Triassic Moenkopi Formation of the southwestern United States. *Journal of the Arizona-Nevada Academy of Science*, *22*, 1–19.

Mundil, R., Ludwig, K. R., Metcalfe, I., & Renne, P. R. (2004). Age and timing of the Permian mass extinctions: U/Pb dating of closed-system zircons. *Science*, *305*(5691), 1760–1763. https://doi.org/10.1126/science.1101012

Nesbitt, S. J. (2003). *Arizonasaurus* and its implications for archosaur divergence. *Proceedings of the Royal Society of London*, *270*, S234–S237. https://doi.org/10.1098/rsbl.2003.0066

Nesbitt, S. J. (2005a). Stratigraphy and tetrapod fauna of major quarries in the Moenkopi Formation (Early-Middle Triassic) along the Little Colorado River of northern Arizona. *Mesa Southwest Museum Bulletin*, *11*, 18–33.

Nesbitt, S. J. (2005b). A new archosaur from the upper Moenkopi Formation (Middle Triassic) of Arizona and its implications for rauisuchian phylogeny and diversification. *Neues Jahrbuch für Geologie und Paläontologie - Monatshefte*, *2005*(6), 332–346. https://doi.org/10.1127/njgpm/2005/2005/332

Nesbitt, S. J. (2005c). The tetrapod fauna of the Moenkopi Formation in northern Arizona. *Mesa Southwest Museum Bulletin*, *9*, 25–32.

Nesbitt, S. J., Barrett, P. M., Werning, S., Sidor, C. A., & Charig, A. J. (2012). The oldest dinosaur? A Middle Triassic dinosauriform from Tanzania. *Biology Letters*, *9*, 1–5.

Nesbitt, S. J., Butler, R. J., Ezcurra, M. D., Barrett, P. M., Stocker, M. R., Angielczyk, K. D., et al. (2017). The earliest bird-line archosaurs and the assembly of the dinosaur body plan. *Nature*, *544*, 484–487. https://doi.org/10.1038/nature22037

Nesbitt, S. J., Liu, J., & Li, C. (2011). A sail-backed suchian from the Heshanggou Formation (Early Triassic: Olenekian) of China. *Earth and Environmental Science Transactions of the Royal Society of Edinburgh*, *101*, 271–284. https://doi.org/10.1017/s1755691011020044

Nesbitt, S. J., Sidor, C. A., Irmis, R. B., Angielczyk, K. D., Smith, R. M. H., & Tsuji, L. A. (2010). Ecologically distinct dinosaurian sister group shows early diversification of Ornithodira. *Nature*, *464*, 95–98. https://doi.org/10.1038/nature08718

Nesbitt, S. J., Zawiskie, J. M., & Dawley, R. M. (2020). The osteology and phylogenetic position of the loricatan (Archosauria: Pseudosuchia) *Heptasuchus clarki*, from the ?mid-Upper Triassic, southeastern Big Horn Mountains, central Wyoming (USA). *PeerJ*, *8*, 1–57, e10101. https://doi.org/10.7717/peerj.10101

Ogg, J. G. (2012). Triassic. In F. M. Gradstein, J. G. Ogg, M. D. Schmitz, & G. M. Ogg (Eds.), *The geologic time scale* (pp. 681–730). Elsevier.

Ogg, J. G., Chen, Z. Q., Orchard, M. J., & Jiang, H. S. (2020). The Triassic Period. In F. M. Gradstein, J. G. Ogg, M. D. Schmitz, & G. M. Ogg (Eds.), *Geologic time scale 2020* (pp. 903–953): Elsevier. https://doi.org/10.1016/b978-0-12-824360-2.00025-5

Olsen, P. E., Geissman, J. W., Kent, D. V., Gehrels, G. E., Mundil, R., Irmis, R. B., et al. (2018). Colorado Plateau Coring Project, phase I (CPCP-I): A continuously cored, globally exportable chronology of Triassic continental environmental change from Western North America. *Scientific Drilling*, *24*, 15–40. https://doi.org/10.5194/sd-24-15-2018

Olsen, P. E., Kent, D. V., & Geissman, J. W. (2008). Climatic, tectonic, and biotic evolution in continental cores: Colorado Plateau Coring Project workshop; St. George, Utah, 13–16 November 2007. *EOS Transactions*, *89*(12), 118. https://doi.org/10.1029/2008eo120003

Ottone, E. G., Monti, M., Marsicano, C. A., de la Fuente, M. S., Naipauer, M., Armstrong, R., & Mancuso, A. C. (2014). A new Late Triassic age for the Triassic Puesto Viejo Group (San Rafael depocenter, Argentina): SHRIMP U–Pb zircon dating and correlations across southern Gondwana. *Journal of South American Earth Sciences*, *56*, 186–199. https://doi.org/10.1016/j.jsames.2014.08.008

Padian, K. (2013). The problem of dinosaur origins: Integrating three approaches to the rise of Dinosauria. *Earth and Environmental Science Transactions of the Royal Society of Edinburgh*, *103*, 423–442. https://doi.org/10.1017/s1755691013000431

Parés, J. M. (2015). Sixty years of anisotropy of magnetic susceptibility in deformed sedimentary rocks. *Frontiers of Earth Science*, *3*, 4.

Parker, W. G. (2006). The stratigraphic distribution of major fossil localities in Petrified Forest National Park, Arizona. *Museum of Northern Arizona Bulletin*, *62*, 46–61.

Payne, J. L., Lehrmann, D. J., Wei, J., Orchard, M. J., Schrag, D. P., & Knoll, A. H. (2004). Large perturbations of the carbon cycle during recovery from the end-Permian extinction. *Science*, *305*(5683), 506–509. https://doi.org/10.1126/science.1097023

Peabody, F. E. (1948). Reptile and amphibian trackways from the Lower Triassic Moenkopi Formation of Arizona and Utah. *University of California Publications, Bulletin of the Department of Geological Sciences*, *27*, 295–468.

Peecook, B. R., Steyer, J. S., Tabor, N. J., & Smith, R. M. H. (2017). Updated geology and vertebrate paleontology of the Triassic Ntawere Formation of northeastern Zambia, with special emphasis on the archosauromorphs. *Journal of Vertebrate Paleontology*, *17*, 8–38. https://doi.org/10.1080/02724634.2017.1410484

Poborski, S. J. (1954). Virgin Formation (Triassic) of the St. George, Utah, area. *The Geological Society of America Bulletin*, *65*(10), 971–1006. https://doi.org/10.1130/0016-7606(1954)65[971:vftots]2.0.co;2

Purucker, M. E., Elston, D. P., & Shoemaker, E. M. (1980). Early acquisition of characteristic magnetization in red beds of the Moenkopi Formation (Triassic), Gray Mountain, Arizona. *Journal of Geophysical Research*, *85*(B2), 997–1012. https://doi.org/10.1029/jb085ib02p00997

Ramezani, J., Bowring, S. A., Pringle, M. S., Winslow, F. D., III, & Rasbury, E. T. (2005). The Manicouagan impact melt rock: A proposed standard for the intercalibration of U–Pb and ^{40}Ar/^{39}Ar isotopic systems. *Geochimica et Cosmochimica Acta*, *69*(10), 321.

Ramezani, J., Hoke, G. D., Fastovsky, D. E., Bowring, S. A., Therrien, F., Dworkin, S. I., et al. (2011). High-precision U-Pb zircon geochronology of the Late Triassic Chinle Formation, Petrified Forest National Park (Arizona, USA): Temporal constraints on the early evolution of dinosaurs. The *Geological Society of America Bulletin*, *123*(11), 2142–2159. https://doi.org/10.1130/b30433.1

Rasmussen, C., Mundil, R., Irmis, R. B., Geisler, D., Gehrels, G. E., Olsen, P. E., et al. (2020). U-Pb zircon geochronology and depositional age models for the Upper Triassic Chinle Formation (Petrified Forest National Park, Arizona, USA): Implications for Late Triassic paleoecological and paleoenvironmental change. *The Geological Society of America Bulletin*. https://doi.org/10.1130/b35485.1

Rayfield, E. J., Barrett, P. M., McDonnell, R. A., & Willis, K. J. (2005). A Geographical Information System (GIS) study of Triassic vertebrate biochronology. *Geological Magazine*, *142*(4), 327–354. https://doi.org/10.1017/s001675680500083x

Rayfield, E. J., Barrett, P. M., & Milner, A. R. (2009). Utility and validity of Middle and Late Triassic 'land vertebrate faunachrons'. *Journal of Vertebrate Paleontology*, *29*(1), 80–87. https://doi.org/10.1671/039.029.0132

Riggs, N. R., Ash, S. R., Barth, A. P., Gehrels, G. E., & Wooden, J. L. (2003). Isotopic age of the Black Forest Bed, Petrified Forest Member, Chinle Formation, Arizona: An example of dating a continental sandstone. *The Geological Society of America Bulletin*, *115*(11), 1315–1323. https://doi.org/10.1130/b25254.1

Riggs, N. R., Lehman, T. M., Gehrels, G. E., & Dickinson, W. R. (1996). Detrital zircon link between headwaters and terminus of the Upper Triassic Chinle-Dockum paleoriver system. *Science*, *273*, 97–100. https://doi.org/10.1126/science.273.5271.97

Riggs, N. R., Sanchez, T. B., & Reynolds, S. J. (2020). Evolution of the early Mesozoic Cordilleran arc: The detrital zircon record of back-arc basin deposits, Triassic Buckskin Formation, western Arizona and southeastern California. *Geosphere*, *16*, 1042–1057. https://doi.org/10.1130/ges02193.1

Rinehart, L. F., Lucas, S. G., & Schoch, R. R. (2015). *Eocyclotosaurus appetolatus*, a new cyclotosaurid amphibian from the Middle Triassic (Perovkan) Moenkopi Formation of New Mexico, USA. *Journal of Vertebrate Paleontology*, *35*(3), e929140. https://doi.org/10.1080/02724634.2014.929140

Romano, M., Bernardi, M., Petti, F. M., Rubidge, B., Hancox, J., & Benton, M. J. (2020). Early Triassic terrestrial tetrapod fauna: A review. *Earth-Science Reviews*, *210*, 103331. https://doi.org/10.1016/j.earscirev.2020.103331

Säilä, L. K. (2008). The osteology and affinities of *Anomoiodon liliensterni*, a procolophonid reptile from the Lower Triassic Bundsandstein [sic] of Germany. *Journal of Vertebrate Paleontology*, *28*(4), 1199–1205. https://doi.org/10.1671/0272-4634-28.4.1199

Schoch, R. R. (2000). The status and osteology of two new cyclotosaurid amphibians from the upper Moenkopi Formation of Arizona (Amphibia: Temnospondyli; Middle Triassic). *Neues Jahrbuch für Geologie und Paläontologie - Abhandlungen*, *216*(3), 387–411. https://doi.org/10.1127/njgpa/216/2000/387

Schoch, R. R. (2011). How diverse is the temnospondyl fauna in the Lower Triassic of southern Germany? *Neues Jahrbuch für Geologie und Paläontologie - Abhandlungen*, *261*(1), 49–60. https://doi.org/10.1127/0077-7749/2011/0147

Schoch, R. R., Nesbitt, S., Müller, J., Lucas, S. G., & Boy, J. A. (2010). The reptile assemblage from the Moenkopi Formation (Middle Triassic) of New Mexico. *Neues Jahrbuch für Geologie und Paläontologie - Abhandlungen*, *255*(3), 345–369. https://doi.org/10.1127/0077-7749/2009/0030

Schultz, C. L. (2005). Biostratigraphy of the non-marine Triassic: Is a global correlation based on tetrapod faunas possible? In E. A. M. Koutsoukos (Ed.), *Applied stratigraphy* (pp. 123–145): Springer.

Shive, P. N., Steiner, M. B., & Huycke, D. T. (1984). Magnetostratigraphy, paleomagnetism, and remanence acquisition in the Triassic Chugwater Formation of Wyoming. *Journal of Geophysical Research*, *89*(B3), 1801–1815. https://doi.org/10.1029/jb089ib03p01801

Shoemaker, E. M., Elston, D. P., & Helsley, C. E. (1973). Depositional history of the Moenkopi Formation in light of its magnetostratigraphy. *Geological Society of America Abstract with Program*, *5*, 807–808.

Sidor, C. A., Smith, R. M. H., Huttenlocker, A. K., & Peecook, B. R. (2014). New Middle Triassic tetrapods from the upper Fremouw Formation of Antarctica and their depositional setting. *Journal of Vertebrate Paleontology*, *34*(4), 793–801. https://doi.org/10.1080/02724634.2014.837472

Sidor, C. A., Vilhena, D. A., Angielczyk, K. D., Huttenlocker, A. K., Nesbitt, S. J., Peecook, B. R., et al. (2013). Provincialization of terrestrial faunas following the end-Permian mass extinction. *Proceedings of the National Academy of Sciences*, *110*(20), 8129–8133. https://doi.org/10.1073/pnas.1302323110

Soreghan, G. S., Keller, G. R., Gilbert, M. C., Chase, C. G., & Sweet, D. E. (2012). Load-induced subsidence of the Ancestral Rocky Mountains recorded by preservation of Permian landscapes. *Geosphere*, *8*(3), 654–668. https://doi.org/10.1130/ges00681.1

Spencer, P. S., & Isaac, K. P. (1983). Triassic vertebrates from the Otter Sandstone Formation of Devon, England. *Proceedings of the Geologists' Association*, *94*(3), 267–269. https://doi.org/10.1016/s0016-7878(83)80045-5

Spencer, P. S., & Storrs, G. W. (2002). A re-evaluation of small tetrapods from the Middle Triassic Otter Sandstone Formation of Devon, England. *Palaeontology*, *45*(3), 447–467. https://doi.org/10.1111/1475-4983.00245

Steiner, M. B. (1986). Rotation of the Colorado Plateau. *Tectonics*, *5*(4), 649–660. https://doi.org/10.1029/tc005i004p00649

Steiner, M. B., & Lucas, S. (1992). A Middle Triassic paleomagnetic pole for North America. *The Geological Society of America Bulletin*, *104*, 993–998. https://doi.org/10.1130/0016-7606(1992)104<0993:amtppf>2.3.co;2

Steiner, M. B., & Lucas, S. G. (2000). Paleomagnetism of the Late Triassic Petrified Forest Formation, Chinle Group, western United States: Further evidence of "large" rotation of the Colorado Plateau. *Journal of Geophysical Research*, *105*(B11), 25791–25808. https://doi.org/10.1029/2000jb900093

Steiner, M. B., Morales, M., & Shoemaker, E. M. (1993). Magnetostratigraphic, biostratigraphic, and lithologic correlations in Triassic strata of the western United States. *SEPM Special Publication*, *49*, 41–57. https://doi.org/10.2110/pec.93.49.0041

Stewart, J. H., Poole, F. G., Wilson, R. F., & Cadigan, R. A. (1972). Stratigraphy and origin of the Triassic Moenkopi Formation and related strata in the Colorado Plateau region. *U.S. Geological Survey Professional Paper*, *691*, 1–195.

Studýnka, J., Chadima, M., & Suza, P. (2014). Fully automated measurement of anisotropy of magnetic susceptibility using 3D rotator. *Tectonophysics*, *629*, 6–13. https://doi.org/10.1016/j.tecto.2014.02.015

Sues, H.-D., & Reisz, R. R. (2008). Anatomy and phylogenetic relationships of *Sclerosaurus armatus* (Amniota: Parareptilia) from the Buntsandstein (Triassic) of Europe. *Journal of Vertebrate Paleontology*, *28*(4), 1031–1042. https://doi.org/10.1671/0272-4634-28.4.1031

Szurlies, M. (2004). Magnetostratigraphy: The key to a global correlation of the classic Germanic Trias - Case study Volpriehausen Formation (middle Buntsandstein), central Germany. *Earth and Planetary Science Letters*, *227*(3–4), 395–410. https://doi.org/10.1016/j.epsl.2004.09.011

Szurlies, M. (2007). Latest Permian to Middle Triassic cyclo-magnetostratigraphy from the Central European Basin, Germany: Implications for the geomagnetic polarity timescale. *Earth and Planetary Science Letters*, *261*, 602–619. https://doi.org/10.1016/j.epsl.2007.07.018

Tarailo, D. A., & Fastovsky, D. E. (2012). Post-Permo-Triassic terrestrial vertebrate recovery: Southwestern United States. *Paleobiology*, *38*(4), 644–663. https://doi.org/10.1666/11054.1

Tarling, D., & Hrouda, F., (Eds.), (1993). *Magnetic anisotropy of rocks*. Springer Science & Business Media

Tauxe, L., Kent, D. V., & Opdyke, N. D. (1980). Magnetic components contributing to the NRM of Middle Siwalik red beds. *Earth and Planetary Science Letters*, *47*(2), 279–284. https://doi.org/10.1016/0012-821x(80)90044-8

Thomson, T. J., & Lovelace, D. M. (2014). Swim track morphotypes and new track localities from the Moenkopi and Red Peak formations (Lower-Middle Triassic) with preliminary interpretations of aquatic behaviors. *New Mexico Museum of Natural History & Science Bulletin*, *62*, 103–128.

Torsvik, T. H., Van der Voo, R., Preeden, U., Mac Niocaill, C., Steinberger, B., Doubrovine, P. V., & Meert, J. G. (2012). Phanerozoic polar wander, palaeogeography and dynamics. *Earth-Science Reviews*, *114*(3–4), 325–368. https://doi.org/10.1016/j.earscirev.2012.06.007

Trotter, J. A., Williams, I. S., Nicora, A., Mazza, M., & Rigo, M. (2015). Long-term cycles of Triassic climate change: A new $\delta^{18}O$ record from conodont apatite. *Earth and Planetary Science Letters*, *415*, 165–174. https://doi.org/10.1016/j.epsl.2015.01.038

von Quadt, A., Gallhofer, D., Guillong, M., Peytcheva, I., Waelle, M., & Sakata, S. (2014). U-Pb dating of CA/non-CA treated zircons obtained by LA-ICP-MS and CA-TIMS techniques: Impact for their geological interpretation. *Journal of Analytical Atomic Spectrometry*, *29*(9), 1618–1629. https://doi.org/10.1039/c4ja00102h

Walker, T. R., Larson, E. E., & Hoblitt, R. P. (1981). Nature and origin of hematite in the Moenkopi Formation (Triassic), Colorado Plateau: A contribution to the origin of magnetism in red beds. *Journal of Geophysical Research*, *86*(B1), 317–333. https://doi.org/10.1029/jb086ib01p00317

Welles, S. P. (1947). Vertebrates from the upper Moenkopi Formation of northern Arizona. *University of California Publications, Bulletin of the Department of Geological Sciences*, *27*(7), 241–294.

Welles, S. P., & Cosgriff, J. (1965). A revision of the labyrinthodont family Capitosauridae, and a description of *Parotosaurus peabodyi*, n. sp. Wupatki Member of the Moenkopi Formation of northern Arizona. *University of California Publications in Geological Sciences*, *54*, 1–148.

Yang, Z., Ma, X., Besse, J., Courtillot, V., Xing, L., Xu, S., & Zhang, J. (1991). Paleomagnetic results from Triassic sections in the Ordos Basin, north China. *Earth and Planetary Science Letters*, *104*(2–4), 258–277. https://doi.org/10.1016/0012-821x(91)90208-y

Zeigler, K. E., Parker, W. G., & Martz, J. W. (2017). The lower Chinle Formation (Late Triassic) at Petrified Forest National Park, southwestern USA: A case study in magnetostratigraphic correlations. *Terrestrial depositional systems* (pp. 237–277). Elsevier. https://doi.org/10.1016/b978-0-12-803243-5.00006-6

Zijderveld, J. D. A. (1967). In D. W. Collinson, K. M. Creer, & S. K. dan Runcorn (Eds.), *A demagnetization of rocks: Analysis of results. Dalam*. Methods in paleomagnetism (pp. 254–286) Elsevier.